5-4-2018

Microfluidic Study of Hydrogen Peroxide (H2O2) Transport Modeled on the MSN-DA Neuron Pathway

Carrie A. Phillips
cap3631@rit.edu

Microfluidic Study of Hydrogen Peroxide (H_2O_2) Transport Modeled on the MSN-DA Neuron Pathway

Carrie A. Phillips

A Thesis Submitted in Partial Fulfillment of the Requirements for the Degree of Master of Science in Mechanical Engineering

Supervised by

Dr. Kathleen Lamkin-Kennard
Department of Mechanical Engineering
Kate Gleason College of Engineering
Rochester Institute of Technology
Rochester, New York
May 4, 2018

Committee Approval:

Dr. Kathleen Lamkin-Kennard — Date
Department of Mechanical Engineering
Thesis Advisor

Dr. Michael Schrlau — Date
Department of Mechanical Engineering
Committee Member

Dr. Lapizco-Encinas — Date
Department of Biomedical Engineering
Committee Member

Dr. Alan Nye — Date
Department of Mechanical Engineering
Department Representative

Abstract

Reactive Oxygen Species (ROS) are produced throughout the body and can cause damage, lead to neurodegenerative disorders, and deactivate neurons involved in the release of essential neurotransmitters. However, the underlying mechanisms affecting neuronal dysfunction are controversial and are not yet well understood. Hydrogen peroxide (H_2O_2), a common ROS, has been shown to inhibit evoked dopamine (DA) in the Nigrostriatal region of the brain. Although unconfirmed, one theory claims that the DA-modulating H_2O_2 is produced in medium spiny neurons (MSN), based on close proximity. However, most literature cites H_2O_2 as a very small molecule which can travel far, diffuse readily, and transport easily between cells. This theory is commonly used when describing ROS damage, but more insight is needed to be able to distinguish mass transport pathways of hydrogen peroxide. The experimental setup used in this research was developed around a sensitive, cost-effective, reliable, solution for detecting H_2O_2. A microfluidic device was designed to simulate the basic geometry of the MSN-DA pathway and was fabricated using 3-D printing. Sample collection and colorimetric analysis was fine-tuned so that a time-dependent analysis of H_2O_2 transport was possible, within the limitations of the system. This work represents a proof-of-concept scenario and information gained can be used for future experiments aimed at predicting H_2O_2 transport within the MSN-DA pathway.

To Ethan, you are my sun, my son.

ACKNOWLEDGMENTS

It is a great honor and pleasure to work with Dr. Lamkin-Kennard. Her optimism, support, and enthusiasm have helped guide me through the development of this study. I admire all of her accomplishments and continuing passion towards the field of engineering.

I'd also like to thank the Mechanical Engineering department for the departmental funding which I received to help me during this work. A special thanks to Dr. Lamkin-Kennard for her extra efforts along with Dr. Robinson and Diane Selleck. All three have gone above and beyond to help, and for this I am deeply appreciative.

Thank you to Dr. Schrlau for allowing me to use the resources in the Nano-Bio Interface Laboratory (NBIL) and to Peter Lamberg for his extensive help with electrochemistry.

Thank you Dr. Lapizco-Encinas for your kind words and support, it means a lot to me that you say I have courage.

Thank you to my family and friends, I couldn't have done it without you…

TABLE OF CONTENTS

LIST OF FIGURES

LIST OF TABLES

NONMENCLATURE

ADHD	= Attention deficit hyperactivity disorder
Ag	= Silver
AMPA	= α-amino-3-hydroxy-5-methyl-4-isoxazolepropionic acid
Ar	= Argon
ATP	= Adenosine triphosphate
CE	= Counter electrode
CO_2	= Carbon dioxide
CV	= Cyclic voltammetry
DA	= Dopamine
GABA	= γ-Aminobutyric acid
GSH Px	= Glutathione peroxidase
H_2O	= Water
H_2O_2	= Hydrogen Peroxide
HRP	= Horseradish Peroxidase
K_{ATP}	= ATP-sensitive potassium channel
MAO	= L-monoamine oxidases
MCS	= mercaptosuccinate
MSN	= Medium spiny neuron
N_2	= Nitrogen gas
NADPH Oxidase	= Nicotinamide adenine dinucleotide phosphate-oxidase (NO_x)
O_2	= Oxygen gas
PBS	= Phosphate buffered saline
PDMS	= Polydimethylsiloxane
Prx	= Peroxiredoxin
Pt	= Platinum
RCA	= Repeated Chronoamperometry
RE	= Reference electrode
ROS	= Reactive oxygen species
S/N	= Signal to noise ratio
SNc	= Substantia nigra pars compacta
SUR	= sulfonylurea receptor
UME	= Ultramicroelectrode
VTA	= Ventral tegmental area
WE	= Working electrode

1.0 INTRODUCTION

Dopamine is associated with reward, motivation, feelings of euphoria, and motor control [1]. Chronic dopamine dysfunction leads to neurodegenerative diseases such as Parkinson's [2, 3] and is implicated in psychological disorders such as bipolar disorder and attention deficit hyperactive disorder (ADHD). Dopamine dysfunction is now associated with more common activities such as internet use [4-6]. Reactive Oxygen Species (ROS), such as hydrogen peroxide (H_2O_2), are well known causes of damage to dopamine neurons [3, 7]. H_2O_2 is also considered to be a signaling agent for cellular communication and has been theorized to decrease the evoked dopamine release of striatal dopamine (DA) neurons [8-13].

The underlying mechanisms affecting dopaminergic neuronal dysfunction are controversial and are not yet well understood. Theories use close proximity, antagonists, and inhibitors to assume that their model is correct, however, physical examination based on mathematical modeling, flow studies, and simulation are lacking, especially regarding the transport between Medium Spiny Neuron (MSN) and DA neuron terminals located in the substantia nigra pars compacta (SNc).

There is a major assumption that the source of dopamine modulating H_2O_2 is from MSNs due to their close proximity to DA neuron terminals. There has been little done to simulate the transport using a mathematical/ physical basis. There is also little evidence of evoked dopamine inhibition beyond the primary evidence from the Rice group of researchers [8-13].

Hydrogen peroxide is a very small molecule (~800 pm) that can diffuse easily across membranes and between cells [13-15]. It is also considered very stable because it is not a free radical and thus can travel long distances away from production sites due to its extended lifetime. However, the primary theory is that the source of modulatory H_2O_2 is from striatal MSNs, due to their close proximity to DA terminals, and contain alpha-amino-3-hydroxy-5methyle-4isoxazole propionic acid (AMPA) receptors [8-13]. This theory discredits that the source may be from striatal cholinergic interneurons, which also contain AMPA receptors, because they are considered too far to have an impact.

This study aims to develop an experimental setup which can be used to observe, document, and analyze the diffusion of H_2O_2. The setup will incorporate a detection method and specially developed fluidic devices. Variations in geometry and spacing of the fluidic devices will simulate transport between MSN and DA neuron terminals located in the SNc, as well as unconstrained and spherical transport. The

insights gained will help quantify H_2O_2 transport and answer questions regarding how geometry and spacing influence H_2O_2 diffusion.

The study should help bridge a gap between theories in biology and physical transport of H_2O_2. Mostly, it will shed light on the commonly accepted theory that the DA-modulating H_2O_2 is from MSNs by helping to characterize its transport. From this, a better sense of how far is "far from diffusion sites", how easily does it "travel easily between cells" and how readily does it "diffuse readily across membranes" could be gained. Not only will it help characterize the diffusion of H_2O_2 from MSN to DA neurons, but the insight gained could extend to H_2O_2 being produced in all cells within the body. The information could also help study pathology of degeneration caused by H_2O_2 by being able to better predict mass transport pathways.

1.1 Motivation

The underlying mechanisms affecting dopaminergic neuronal dysfunction are controversial and are not yet well understood. Theories use close proximity, antagonists, and inhibitors to qualitatively assume that their model is correct, however, quantification based on mathematical modeling, flow studies, and simulation are lacking, especially regarding the transport between Medium Spiny Neuron and dopaminergic neuron terminals located in the substantia nigra pars compacta (SNc) [8-13].

Major questions stem from the assumption that the source of dopamine modulating H_2O_2 is from MSN due to their close proximity to DA neuron terminals. There has been little done to quantitatively assess the diffusion across the MSN-DA channel. There is also little evidence of evoked dopamine inhibition beyond the Rice group of researchers [8-13]. A closer examination of H_2O_2 transport should help gain a better understanding of the amount of H_2O_2 that would potentially reach the DA terminal and how long it would take.

This study aimed to develop an experimental setup which can be used to observe, document, and analyze the diffusion of H_2O_2. The setup incorporates a detection method and specially developed fluidic devices. Variations in geometry and spacing of the fluidic devices simulate transport between MSN and DA neuron terminals located in the SNc.

The study may help bridge a gap between theories in biology and physical transport of H_2O_2. Mostly, it will shed light on the commonly accepted theory that the DA-modulating H_2O_2 is from MSNs by helping to characterize its transport. From this, a better sense of how far is “far from diffusion sites”, how easily does it “travel easily between cells” and how readily does it “diffuse readily across membranes”. Not only does it help characterize the diffusion of H_2O_2 from MSN to DA neurons, but the insight gained could extend to H_2O_2 being produced in all cells within the body. This information could help study pathology of degeneration caused by H_2O_2 by being able to better predict mass transport pathways.

1.2 Research Goals

Literature cites H_2O_2 as a very small molecule (~800 pm) that can diffuse easily across membranes and between cells [13-15]. It is also considered very stable because it is not a free radical and thus can travel long distances away from production sites due to its extended lifetime. However, the primary theory is that the source of modulatory H_2O_2 is from striatal MSNs, due to their close proximity to DA terminals, and contain AMPA receptors [8-13]. This theory discredits that the source may be from striatal cholinergic interneurons, which also contain AMPA receptors, because they are considered too far to have an impact.

To gain a better sense of the transport of H_2O_2, this study aims to develop an experimental setup to help examine and quantify H_2O_2 transport within a laboratory setting. The setup focuses on using an effective method to detect H_2O_2 within a flow device modeled around the geometry of the MSN-DA neuron pathway. Mainly, how can the transport of H_2O_2 be examined and quantified within a laboratory setting?

1. Which detection method offers a sensitive, cost-effective, reliable, solution for detecting H_2O_2?
2. What are the input parameters to obtain an appropriate detection signal and range?
3. How can the detection method be calibrated to ensure valid detection?
4. How can devices be fabricated rapidly, cost-effectively, and reliably?
5. How can the detection method be used to measure specific samples?

These questions were approached by determining a detection method and input parameters to obtain an appropriate detection signal and range. The input parameters and detection method were then calibrated to evaluate their effectiveness and reliability. Device fabrication was developed so that the flow device is rapid, cost effective and reliable. A sample collection and detection process was then developed so that the time-dependent analysis of H_2O_2 transport is possible using the chosen device and detection method.

Once the sample collection and detection process was developed, a flow study setup to simulate the MSN-DA pathway was employed to quantitatively analyze the transport within the system. In this part of the process a flow device design was based on the geometry of MSN-DA pathway. The geometric features of this pathway were determined and assessed in order to incorporate into the device based on the chosen fabrication method. Lastly, diffusion based studies were conducted and a time-dependent analysis of the H_2O_2 transport within the system was obtained. Data analysis focused primarily on the diffusion towards the “DA neuron” and a comparison was made to the transport away from this area.

1.3 Literature Review

Dopamine: Pathway and function

Dopamine is associated with reward, motivation, feelings of euphoria, and motor control [1]. Chronic dopamine dysfunction leads to neurodegenerative diseases such as Parkinson's [2, 3] and is implicated in psychological disorders such as bipolar disorder and ADHD. Dopamine dysfunction is now being found in more common activities such as internet use [4-6]. Reactive Oxygen Species (ROS), such as H_2O_2, are well known causes of damage to dopamine neurons [3, 7]. Hydrogen Peroxide is also considered to be a signaling agent for cellular communication, and has been theorized to decrease the evoked dopamine release of striatal dopamine (DA) neurons [8-13].

The substantia nigra pars compacta (SNc) is one of the most abundant sources of DA neurons [16].This projection establishes one of the major dopaminergic pathways, referred to as the Nigrostriatal Pathway [16-18], depicted in Figure 1. Disruption to this pathway leads to a deprivation of dopamine released to the striatum, which can also lead to the loss of SNc-DA neurons [16]. Loss of motor control and slowness of movement, seen in Parkinson's disease, is attributed to degeneration of SNc DA neurons [16, 17].

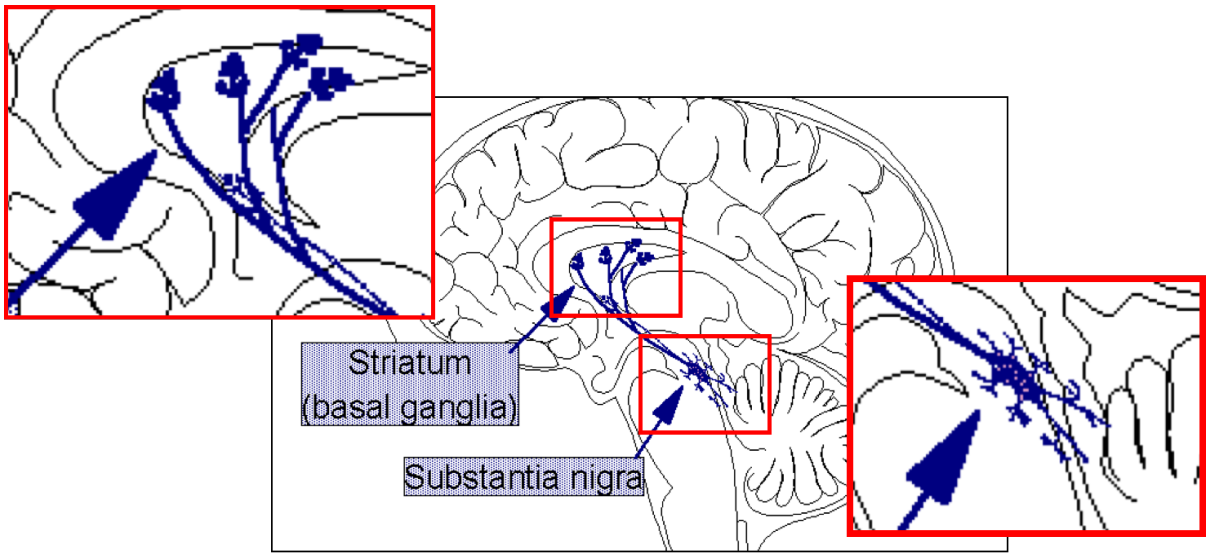

Figure 1: Nigrostriatal Pathway, adapted from: http://163.178.103.176/temas/temab2n/aportal/fisonercg/fisonerob5/parkinson/dopamina/dopamine.htm#mesolimb.

The SNc projects onto the striatum, where DA terminals are distributed ubiquitously [17], and form synapses with Medium Spiny Neurons (MSNs) [18], depicted in Figure 2.

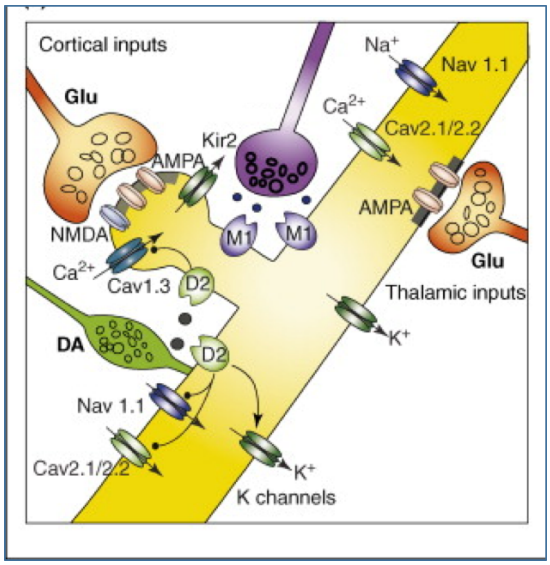

Figure 2: Illustration of a striatal MSN (yellow) creating synapses with DA neuron terminal (green), and glutamate synapse (red)[19].

SNc DA neurons are extremely vulnerable to degeneration, more so than the DA neurons of the ventral tegmental area (VTA) [19], which is the other leading source of DA neurons [16]. The SNc DA neurons exhibit basal pacemaker activity, which increases cellular energy demands [10]. To compensate for higher energy demands, these neurons develop larger axonal arborization [19] which are densely populated with mitochondria, responsible for producing energy[16]. However, mitochondrial energy production also produces CO_2 and H_2O byproducts that can transform into ROS, including H_2O_2. The high baseline rate of oxidative stress is near the maximum capacity seen in these neurons, and is theorized to increase their vulnerability towards degeneration [19]. There is also evidence that extracellular H_2O_2 produced in MSNs may lead to decreased striatal dopamine release [8-13], which may also contribute to degeneration [16].

H_2O_2: Origin, properties

Hydrogen peroxide is a small molecule [13-15] produced by the aerobic metabolism of mitochondrial respiration, throughout the body [13, 14]. According to the literature its small size allows it to travel between cells easily [15] and diffuse across membranes [14]. The lifetime of H_2O_2 is prolonged because it

is not a free radical, and therefore less reactive [15]. It is commonly referred to as being able to diffuse long distances, relative to production sites.

Hydrogen peroxide has also been shown to be a cellular signaling agent, inhibiting firing rates in dopaminergic neurons [8-10, 13]. Although the exact source of modulatory H_2O_2 is undetermined [12], Rice group literature cites extensive studies to localize its effects [8-13]. Their general consensus is that glutamate, acting on AMPA receptors of MSNs, produces the H_2O_2 that decreases the dopamine release of SNc DA neurons. These results were obtained through several experiments using inhibitors and antagonists in order to isolate where the effects of H_2O_2 were occuring. When H_2O_2 metabolism was inhibited, there was a 40% decrease in evoked dopamine [8], whereas inhibition of AMPA receptors caused a 100% increase, and $GABA_a$ antagonists caused a 50% decrease. AMPA and GABA receptors both accept glutamate (or GABA from glutamate [16]), their conflicting effects on dopamine release reveals that they are competing for the same glutamate, which when received by AMPA receptors, creates a H_2O_2 byproduct that can have downstream effects on dopamine release [8]. A schematic of these results is shown in Figure 3.

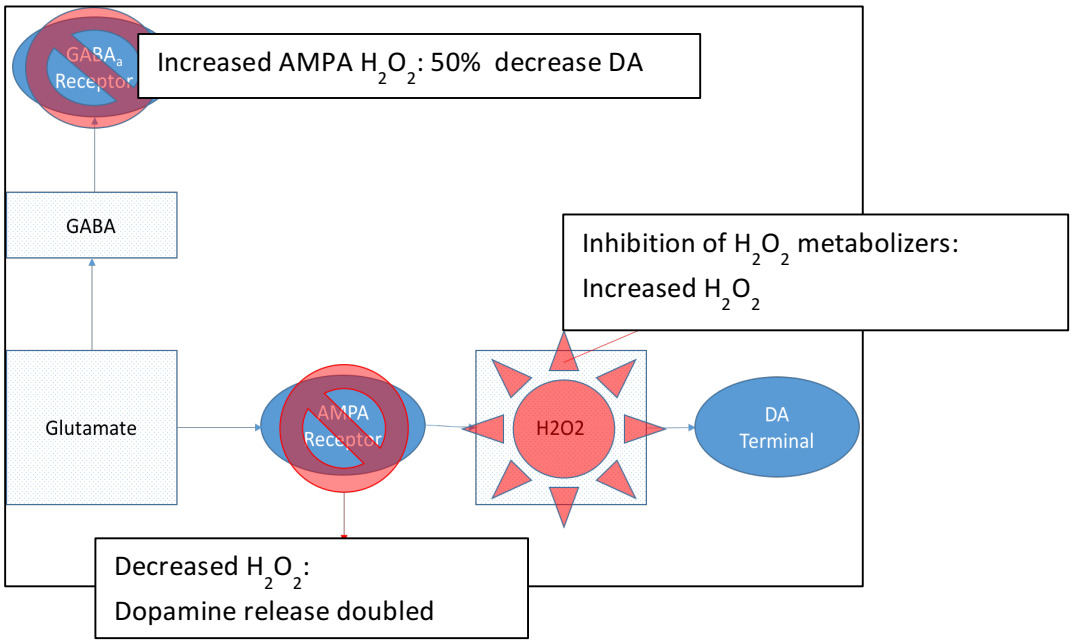

Figure 3: Depiction of Glutamate-AMPA-DA Terminal pathway of H2O2 production/ modulation, based on findings from Rice research group. Original

Modulating mechanism

Activation of ATP-sensitive Potassium Channels (K_{ATP}), located on DA neurons, has been shown to decrease dopamine release [8]. K_{ATP} are normally closed channels, which open when hyperpolarized. The theory is that activation signals a high metabolic demand to the neuron, and therefore shuts down cellular processes in order to conserve energy. When the channels are blocked (kept closed), the modulating effects of H_2O_2 were not seen [8]. Instead there was a 60% increase in dopamine firing, even though there was a steady increase of intracellular H_2O_2 during striatal stimulation, reaching its maximum after the stimulation ended. There was also a difference when using SUR-1 and SUR-2 openers, which are subunits to K_{ATP} channels. Channel activation by H_2O_2 occurred only via SUR-1 receptors. The findings indicate that DA modulation occurs when H_2O_2 activates K_{ATP} channels via SUR-1 receptors.

DA-modulating H_2O_2 source

The primary supporting evidence that indicate MSN as the source for DA modulating H_2O_2 is because of the close proximity to DA terminals, which do not, themselves, contain AMPA receptors, and which contain very few $GABA_a$ receptors [8]. The diffusion from MSN post-synaptic sites to presynaptic DA terminals would only be a few microns. Cholinergic interneurons also contain AMPA receptors, but are not located near DA terminals. Rice et al. concludes that the H_2O_2 generated at Cholinergic AMPA receptors could not possibly transport to DA K_{ATP} channels. The conclusion disregards information that the H_2O_2 can travel long distances because of the molecule's small size and lack of reactivity [13-15]. H_2O_2 is generated through mitochondrial respiration, but can also arise from monoamine oxidase (MAO) and NADPH (Nox) [12]. MAO and Nox form H_2O_2 through two and one electron reductions of O_2, respectively. MAO, in particular, works directly on dopamine. Through the use of MAO inhibitors, there was no change in DA firing, and no significant change with Nox inhibitors. However, when mitochondrial H_2O_2 was inhibited, there was no decrease in evoked dopamine. It was therefore concluded that the source of H_2O_2, that modulates the DA firing, was from mitochondrial respiration. The findings, alongside their previous work [8] point to MSN mitochondria as the specific production site of DA-neuron modulating H_2O_2.

Compared to a control group, evoked DA has been shown to double when AMPA receptors are blocked, indicating that H_2O_2 suppresses even baseline DA [8, 9]. The effect is further increased using H_2O_2 metabolizing inhibitors such as MCS and Catalase. MCS inhibits the effects of glutathione peroxidase

(GSH Px), which reduces H_2O_2 to H_2O. Catalase depletes intracellular H_2O_2, which is produced even during normal pacemaking activity of SNc DA neurons. The inhibition of catalase, which is typically responsible for intracellular consumption of H_2O_2, rapidly increases the amount of intracellular H_2O_2. During the inhibition of catalase, all dopamine neurons were hyperpolarized but during MCS inhibition of GSH, only 50% were hyperpolarized. The findings lead to two ideas: H_2O_2 needs to be at a certain amount, and even at this amount, the effects of H_2O_2 on DA firing are not always seen. Through the use of H_2O_2 metabolizing inhibitors (i.e. catalase and MSC), antagonists (GABA blocking), or application of exogenous H_2O_2, the levels of H_2O_2 become unnaturally elevated and therefore the results may be skewed.

DA-modulating H_2O_2 transport

H_2O_2 is produced in all cells during metabolism [12], but in order to see the effects of DA firing, AMPA receptors must be activated. This implies glutamate dependent H_2O_2 generation [10] and a concentration threshold is suggested. The H_2O_2 minimum seems to be 1.5mM, when applied exogenously, however not all cells respond to elevated levels. About 53% of DA neurons responded to this level, applied exogenously, and only slightly more (~57%) responded with MCS (an H_2O_2 metabolizing inhibitor). While this suggests a threshold of H_2O_2 to elicit inhibitory effects on DA neurons, it also raises questions regarding the efficacy of H_2O_2 to modulate DA neurons. The deficiency may be due to transport problems and accessibility.

If the source of H_2O_2 is from MSN mitochondria to DA terminals [8-10], the transport distance would only be a few microns [9]. The small size of the molecule [15] and its extended lifetime, due to decreased reactivity[13], make it easier for H_2O_2 to travel long distances. However, H_2O_2 transport across membranes [15] and through cytoplasm [20] is not agreed upon. Transport of extracellular H_2O_2 across the biomembrane may be facilitated by aquaporins [13], but others claim that diffusion through the cytoplasm is extremely limited. In these cases it is theorized that transport to these targets may be aided by intracellular gradients, hyperoxidation, and redox relays [20] or that H_2O_2 production sites and targets reside within the same cell [15]. A major component to consider with regards to H_2O_2 transport into a neuron is the plasma membrane. The plasma membrane is around 8-10 nm thick and controls transport with its selective permeability [16].

A major barrier against H_2O_2 penetration into the cell is the abundance of peroxiredoxins, which react with H_2O_2 several orders of magnitude quicker than H_2O_2 reacts with its targets [20]. Peroxisomes

detoxify and protect neurons from H_2O_2 [16]. This is done through catalase, which reduces the H_2O_2 to H_2O.

Simulations by Travasso et al. examined H_2O_2 penetration at various concentrations of extracellular H_2O_2 and fixed amounts of peroxiredoxin [20]. At 0.4 μM H_2O_2, the concentration decayed rapidly as it reacted with the peroxiredoxin, and the diffusion length into the cell was ~0.6 μm, and only ~0.27 μm when a cytoplasm diffusion constant was considered. During pulse simulation of H_2O_2 (extracellular concentration ~0.75 μM), the peroxiredoxin was significantly oxidized and therefore H_2O_2 could penetrate deeper. During stronger pulses, creating ~5.9 μM of extracellular H_2O_2, the simulation hyperoxidation and thus even deeper H_2O_2 penetration exhibited hyperoxidation. At 12 μM extracellular H_2O_2, there was a "hyperoxidation catastrophe", where all peroxiredoxin has been oxidized, and can no longer react with the H_2O_2.

It should be noted that these simulations [20] allowed for permeation across the entire membrane, when in reality they would be limited to channels with diameters around 50 nm. Also, H_2O_2 sinks other than an effective peroxiredoxin, combining Prx I and Prx II, were neglected. Based on these assumptions, the critical amount of H_2O_2 necessary to diffuse would increase. Altogether, most of the H_2O_2 from extracellular sources is limited to fractions of a micron due to cytoplasmic restrictions. However, the authors indicate that the signal caused by redox may be relayed by proteins [20], which are located within the plasma membrane [16].

When looking at HeLa and NIH-3T3 cells, Mishina et. al found H_2O_2 localizing micro-domains within the cytoplasm and limited diffusion of H_2O_2 from production sites [15]. The real-time dynamics of intracellular H_2O_2 were recorded using immobilized HyPer to obtain a clearer representation of what was happening spatial-temporally (Figure 4). They noted that the H_2O_2 does not diffuse freely within the cytoplasm, but instead acts locally within larger pools or "microdomains". Their results concluded that the diffusion within the cell is limited to about a few micrometers, and is most likely degraded before reaching other cellular compartments. However, the plasma membrane may be a target site for extracellular H_2O_2.

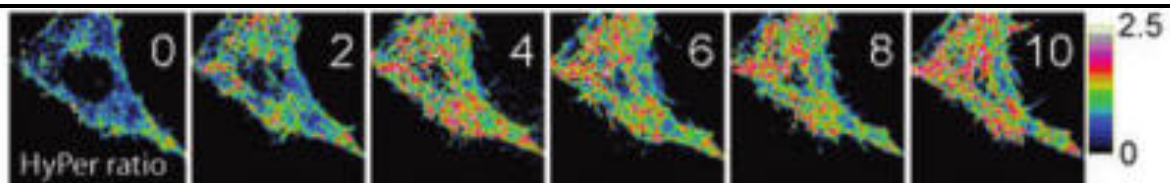

Figure 4: Localized "microdomains" of H_2O_2 (intensity scale indicates amount of H_2O_2, proportional to concentration) within the cytoplasm of a HeLa-Kyoto cell, detected using immobilized HyPer, genetically encoded probes [15].

It should be noted that when mitochondrial K_{ATP} channels were inhibited, there was no typical increase of dopamine release as seen when AMPA receptors were blocked [8], which would indicate involvement of intracellular K_{ATP} mitochondrial respiration, rather than extracellular H_2O_2 (i.e. from MSNs). However, these studies were from different cell lines, so it is important to consider unique transport abilities to specific cells, in this case the MSN for diffusion out of the membrane and the DA neuron for diffusion into the membrane.

Microfluidics

Microfluidics has emerged as a means to be able to work with, analyze, and synthesize fluids at a molecular level [21]. With a decrease in size (channels with10-100 micron diameters), came a decrease in several other aspects such as cost (for both fabrication and employment of the devices), analysis time, required samples/ reagents, and a decrease in waste (of both the sample and the device), which make microfluidics appealing. The other benefits of microfluidics were the increase in resolution, sensitivity, and throughput, beneficial for any analyses completed using microfluidics.

The manufacturing material of the devices has changed over the years, facilitating the field's widespread growth [21]. Originally devices were made of glass and silicon which were expensive and timely to create. These materials were replaced by plastics (a cheaper and quicker option) and also by polydimethylsiloxane (PDMS). PDMS is attractive to exploratory fields because it is inexpensive, easily accessible, and quickly fabricated—with little to no special training required.

Overall, the development of microfluidics has revolutionized fields by allowing for faster, cheaper, less wasteful, more remote analysis and synthesis of fluidics at the molecular level. As the field continues to grow, the applications and abilities are sure to reach further and further.

2.0 Simulation of H_2O_2 Transport in the MSN-DA Pathway

2.1 Introduction

A flow device was designed to represent the geometry of MSN-DA pathway. The most significant geometric features of the pathway were incorporated into the device.

2.2 Geometry of MSN-DA transport pathway

The components of the MSN-DA transport pathway incorporated into the microfluidic device are outlined in Table 1. The dimensions of the device were scaled to simplify the fabrication methods.

Table 1: Significant geometric features of MSN-DA pathway.

Component	Dimension	Significance
Channel width	~3μm	Gap between MSN and DA neurons
Height	~15μm	Diameter of an MSN, 15 μm>>50 nm
Outlet diameter	~50nm	DA neuron channel diameter, although aquaporin diameters~.3 nm

2.3 Device fabrication

Several possibilities offer rapid, cost-effective and reliable methods for fabrication of micro-fluidic devices. The device can either be created in a one-step or two-step method. The one-step method involves cutting into the material of choice and using it as the flow channel. In a two-step method, a mask is produced which can then be poured with a secondary material which becomes the flow channel. Several options for materials and fabrication are available for both methods.

Both one-step and two-step methods were investigated and devices were developed using polystyrene, Shrinky Dinks ™, PDMS, and 3-D printing. Although the minimum feature sizes (~1.2 mm) that can be created with 3-D printing are larger than what can be fabricated using Shrinky-Dinks, it is a quick, inexpensive, and available method to create devices. Also, after shrinking, polystyrene Shrinky Dinks deformed and created gaps in the channels.

3D printing was first used to fabricate a mask that was used to mold PDMS. The printing worked well for the mask. But adhering the PDMS to a glass plate using the plasma gun proved problematic. This was most likely due to the ridges from the 3D printing creating uneven surfaces.

Due to accessibility and ease of use, the device was redesigned to be 3-D printed, in a one-step method, rather than creating a PDMS mold. The final design was an open device which allowed for easier sampling, the ability to clean and reuse, and potentially less back pressure due to being open to the atmosphere.

The device (Figure 5) was designed in SolidWorks TM. The reservoir (#1) was made to be sufficiently large so that samples could be assumed to have negligible effects on the overall volume. In order to achieve the tightest openings into the reservoir and inlet (#3), and maintain structural integrity of the walls, a lachrymiform (tear-drop shape) was used. The open design facilitated sample collection in multiple locations throughout the device such as the side (#2) and channel center (#4). It was then 3-D printed out of polylactic acid (PLA) on a FlashForge Creator Pro printer. The printer was set to CuraFine with 100% fill. Although the printing was not true to the SolidWorks design, actual dimensions were measured and are shown in Figure 6 and listed in Table 2. The depth of the device was 1.5 mm.

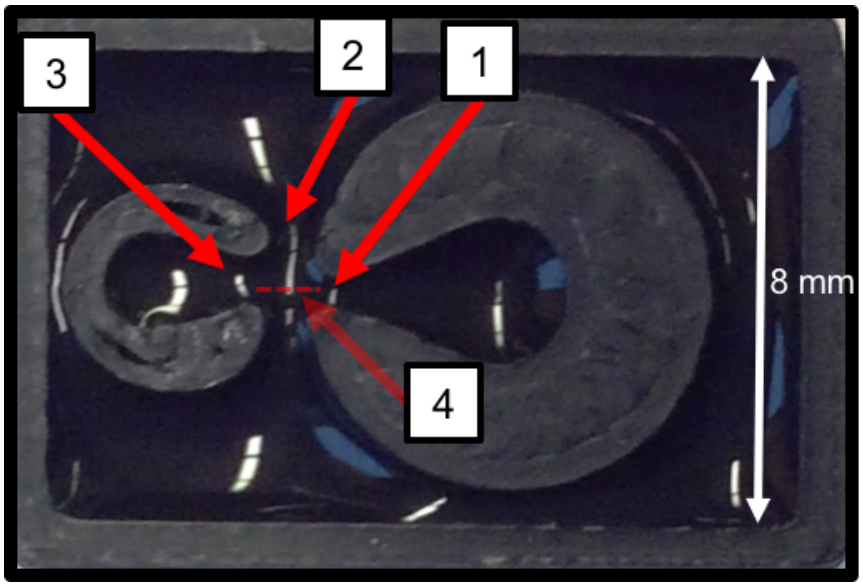

Figure 5: 3-D printed device used in experimentation. 1: "Reservoir", simulating the DA-neuron terminal, 2: "Side", 3: "Inlet", simulating the MSN, 4: "Channel".

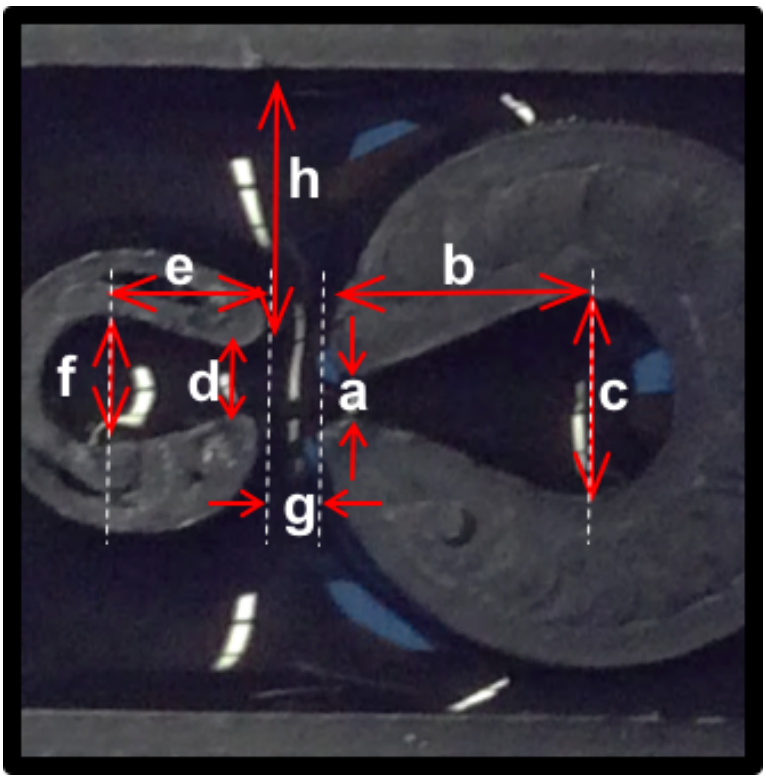

Figure 6: Device with dimensions labeled

Table 2: Actual dimensions of 3-D printed device.

Variable	Description	Length
a	Reservoir opening	2/64”
b	Outside perimeter to largest width (reservoir)	8/64”
c	Largest width of reservoir	6/64”
d	Inlet opening	3/64”
e	Outside perimeter to largest width (inlet)	4/64”
f	Largest width of inlet	4/64”
g	Channel width	3/64”
h	Distance from mid-wall of inlet to device wall	8/64”

3.0 Experimental Setup to Quantify H_2O_2 Transport

3.1 Introduction

To gain a better sense of the transport of H_2O_2 an experimental setup was developed to help examine and quantify the transport within a laboratory setting. The setup focuses on using an effective method to detect H_2O_2 within a flow device modeled around the geometry of the MSN-DA neuron pathway.

Two detection methods, electrochemistry and colorimetry, were attempted and a sample collection and detection process was developed. The appropriate detection method was used in conjunction with the collection process so that the time-dependent analysis of H_2O_2 transport was possible. A flow study setup to simulate the MSN-DA pathway was employed to quantitatively analyze the transport within the system using the fabricated device.

3.2 Sample collection and detection (general concept)

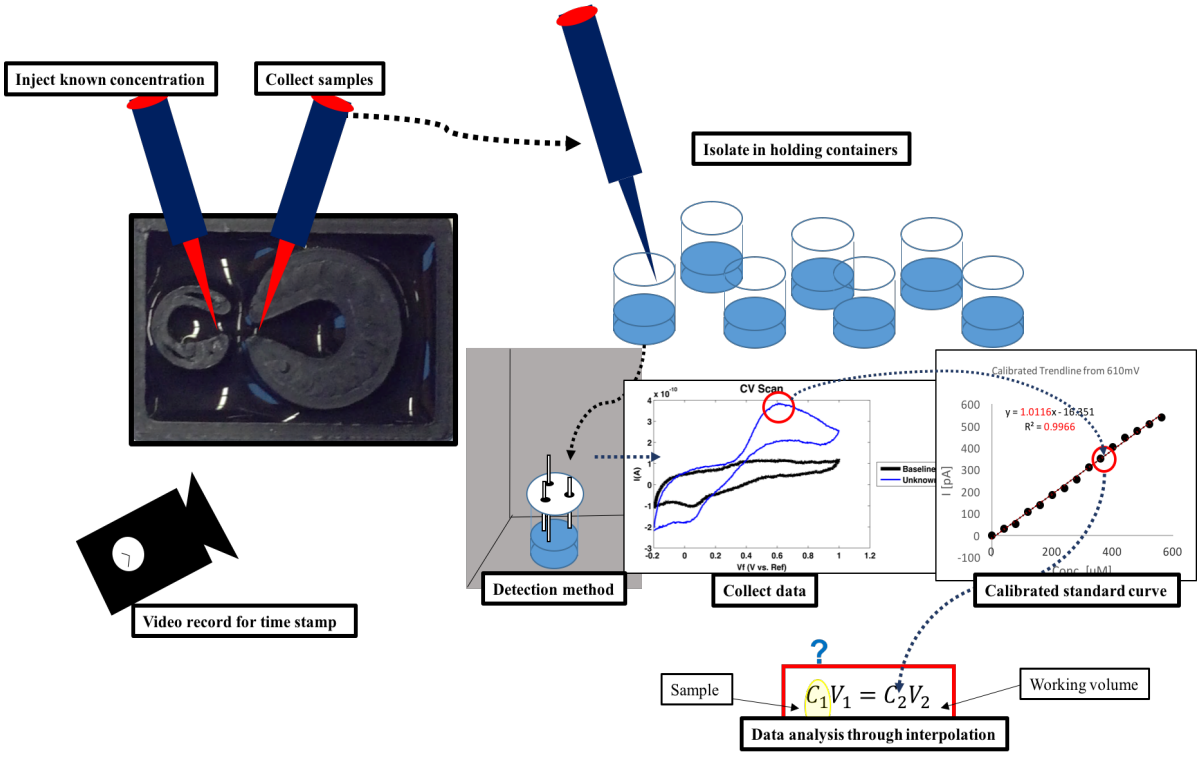

Figure 7: General concept for sample collection and detection for data analysis.

The general concept for the experiment is as follows: pipette samples of known concentration into the inlet, allow to diffuse freely through the channel, and pipette out from the reservoir (Figure 7). Each extracted sample is isolated into a holding container for the remainder of the extraction process. The experiment is video recorded to preserve time-stamps of when each sample is extracted. Once all samples have been obtained, each individual sample is analyzed using a detection method to collect data on the amount of H_2O_2 present in each sample. This data is compared to a calibrated standard curve relating the measure of detection (i.e. current or absorbance) to the amount present. Data analysis involves relating the amount present to sample volumes and working volumes and correlating the time-stamps to examine the transient response of the H_2O_2 transport from the inlet (MSN) to the reservoir (DA-neuron). Experiments pertaining to the channel center and side are also performed for comparison.

3.3 Detection method

Electrochemistry and colorimetry were both investigated as potential detection methods. Sample concentrations were obtained using cyclic voltammetry and chronoamperometry, however, repeatability proved problematic. Thus, the detection method was changed to colorimetry. Both methods are described in detail below.

3.2.1 Electrochemistry

There are several types of H_2O_2 detection methods including electrochemiluminescence [22] and spectrometry [23], but amperometric methods offer a simple, reliable, and quick approach [24-26]. The development of miniaturized electrochemical detection for biological substances dates back to 1967, with the development of "The Enzyme Electrode" [27]. This biosensor was developed by Updike and Hicks as a way to monitor glucose. It employed a microscale (<25 μm) platinum (Pt) electrode with an immobilized enzyme, glucose oxidase, which reacted with glucose and oxygen to produce gluconic acid and H_2O_2. Measured electrochemically, the response could then be correlated to the amount of glucose because it was directly proportional. Since then, many advancements have been made in the development of electrochemical detection methods, but the same basic principles remain.

Setup

A 3-electrode electrochemistry setup was initially chosen as the detection method. A typical 3-electrode system requires a working electrode (WE), counter electrode (CE), and a reference electrode (RE) [26].

For H_2O_2 detection, the WE and CE are typically platinum (Pt), while the RE is silver (Ag). The WE is responsible for catalyzing the H_2O_2 by supplying a voltage to the solution. At low levels of H_2O_2 (<1 mM), the 2 electron oxidation of H_2O_2 produces a current proportional to the amount of H_2O_2 being catalyzed as seen in the following reaction:

$$H_2O_2 \overset{Pt}{\rightarrow} O_2 + 2H^+ + 2e^- \quad [1]$$

While Pt is the traditional choice for the catalyzing metal (WE) and CE, other transition metals also offer great catalytic capabilities [25]. However, Pt electrodes are extremely stable, highly selective and sensitive, and are biocompatible [26]. The chosen setup consisted of a bare platinum ultramicroelectrode (UME) (10 μm diameter) working electrode (WE), a silver-silver chloride (Ag/AgCl) reference electrode (RE) and a platinum wire counter electrode (CE). An UME, which is characterized as having dimensions between 1-25 μm [28], extends the detection possibilities of H_2O_2. These electrodes are highly sensitive and exhibit excellent Signal to Noise ratios (S/N), allowing for the detection of much smaller amounts of H_2O_2 than larger sized electrodes [25]. The highly stable electrodes are also readily available, relatively inexpensive, and require no enzymes, mediators, or immobilization techniques [25, 28]. The working volume was held in an electrochemical cell and the electrochemistry experiments were conducted inside of a Faraday Cage to block outside interference. Nitrogen was used as purging gas to help eliminate oxygen build up on the electrodes. The electrochemical setup is seen in Figure 8.

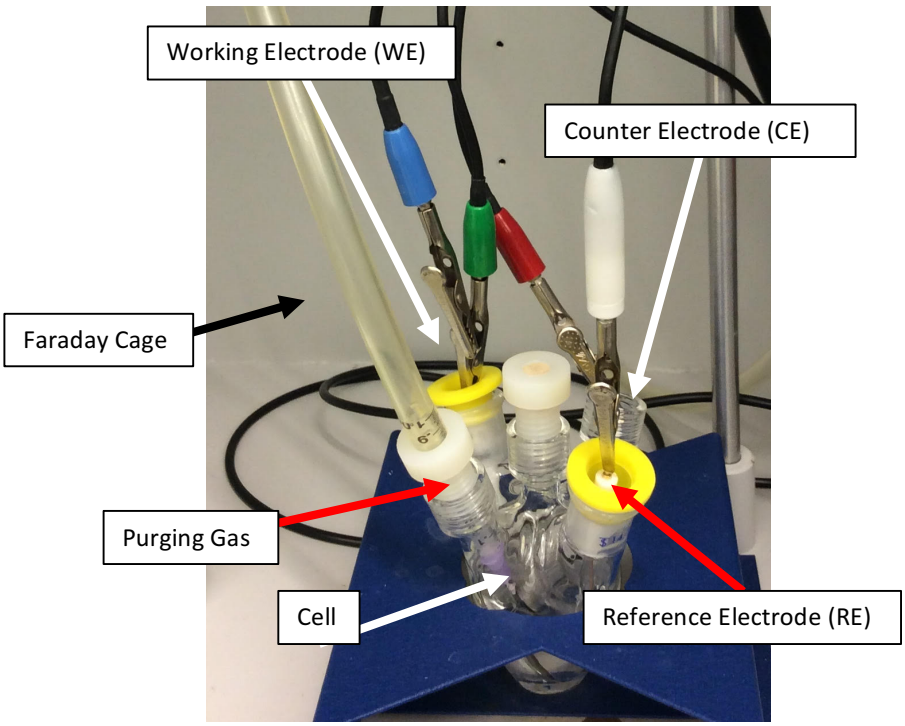

Figure 8: Electrochemistry setup.

Method

Cyclic Voltammetry was used to determine the effectiveness of a 10 µm, bare platinum working electrode (WE) for detection of different concentrations of H_2O_2. A 3-electrode setup was chosen, consisting of an Ag/Cl reference electrode (RE) and Pt wire counter electrode (CE). The scan was conducted in an electrochemical cell, and isolated in a Faraday cage to block outside interference. The working volume contained 22 mL PBS, pH 7.2. The stock solution was prepared by diluting 30% H_2O_2 100X into a separate source of the same PBS. The large dilution allowed for more accurate pipette transfer. Nitrogen gas was used to degas the cell between each scan, preventing ambiguous signals due to oxygen.

Cyclic Voltammetry (CV) is a convenient and effective way to detect H_2O_2 by measuring current at a range of potentials. The current at the peak of the forward scan of the cycle is proportional to the amount of H_2O_2 present in the working solution. Thus the peak of the cycle (the limiting current) can be extracted to obtain the current per concentration slope. Then interpolation can be used to deduce the unknown concentration of a sample by using the measured current.

Input parameters

Several parameters can affect the signal and amount of time it takes to conduct CV scans. Scan rate, step size, and scan range are important parameters to examine in order to obtain an appropriate detection signal and range. An increase in scan rate will give higher peaks and faster scans but also increased noise and could possibly hurt the electrodes. Step size can help filter out noise, and a faster scan rate can be used in conjunction with a high step size to obtain clearer results. The scan range is defined by the initial, maximum, and final potentials of the scan. It is important to consider in order to be able to detect the H_2O_2 by using the correct scan range.

The typical range for H_2O_2 (in degassed PBS) on a bare Pt UME is -0.2 V to 1 V, with the optimal peak occurring at ~0.6 V. CV scanning is performed on a range of concentrations, to determine the detection limits based on whether a peak is detectable at such concentration. It is also important to determine whether the peak increases proportional to the increasing concentration, which indicates that it is due to the H_2O_2 and not another reaction (from oxygen, for example). Some parts of the cycle converge, while the peak from the H_2O_2 reaction (occurring at ~0.6 V) should increase linearly with an increasing concentration of H_2O_2. If the concentration is too low, there will not be an observable peak in the cycle, indicating that detection is not possible.

The scan range used was -200 to 1000 mV and the limiting current peak occurred around 610 mV. Experimentation with shorter cycles showed that the full range (-200 to 1000 mV) is necessary to obtain accurate cycles of H_2O_2. Scans were performed using a variety of scan rates and step sizes to determine which would provide clear signals, minimize noise, and minimize scan time. The initial conclusion was to perform scans at -0.2 V to 1 V, scan rate=20 mV/sec, and step size=2. These parameters allowed for minimal signal to noise ratios and sufficiently high peaks.

Calibration

An essential step in using electrochemistry as the detection method is to initially calibrate the electrodes to determine the slope of current per concentration. This enables concentration in an unknown sample to be correlated to a measured current. A cumulative study was performed starting at baseline (no H_2O_2) and then adding concentrations of H_2O_2 before each scan. The entire study ranged from 2 μM to 400 μM H_2O_2. The study showed consistent increases in current, proportional to H_2O_2 concentration. There was also clear convergence ~200 mV, indicating the increase and peak is due to the H_2O_2. A trendline

obtained from measured currents at 610 mV, at different concentrations, had a near perfect linear fit (R^2=0.9939), indicating good linear proportionality between measured current and H_2O_2 concentration. Results are shown in Figures 9 and10. Data from return scans have been removed for clarity. There was clear convergence ~200 mV, indicating the increase and peak is due to the H_2O_2.

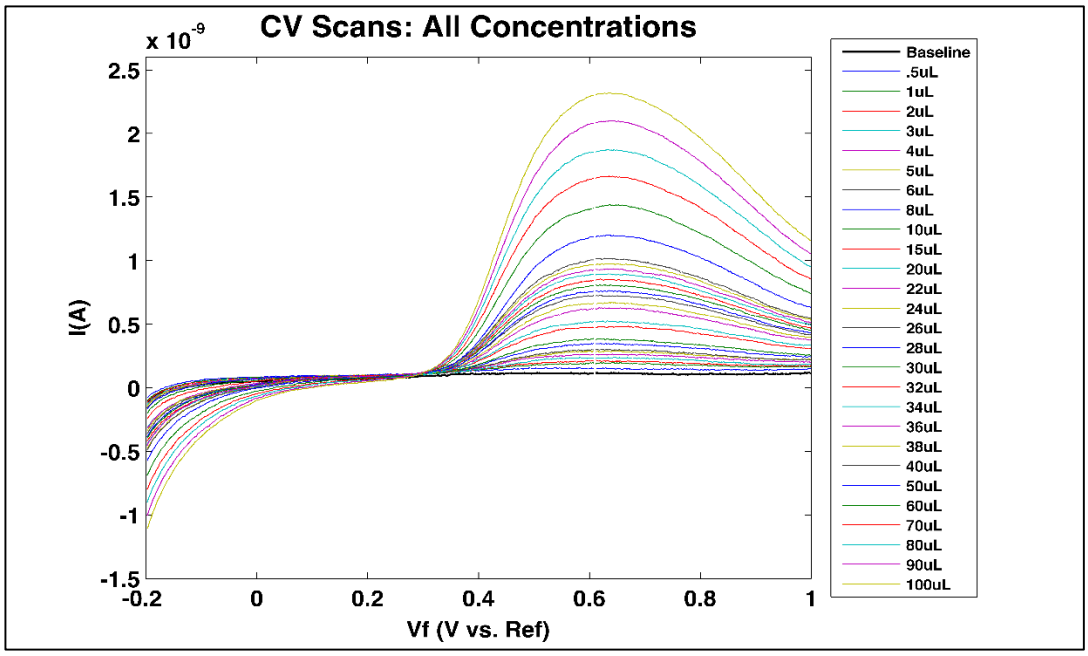

Figure 9: CV scans of all concentration levels, from Baseline (0) to 400 µM.

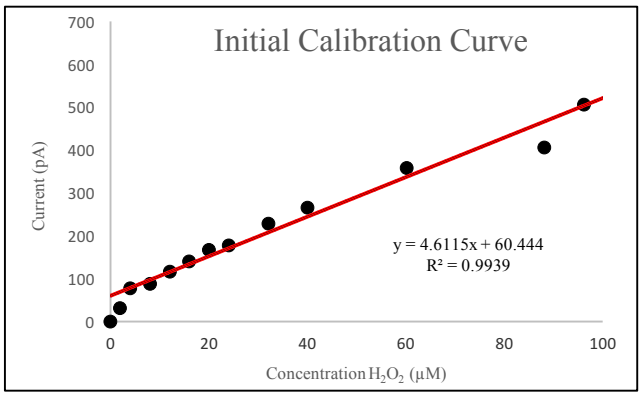

Figure 10: Initial calibration curve for cyclic voltammetry.

Chronoamperometry

After initial success with CV, chronoamperometry was performed to measure current corresponding to each concentration. Chronoamperometry is conducted using the potential at which the peak occurs during CV. During chronoamperometry, this potential is held constant and the current is measured. As H_2O_2 is

added the current increases until steady state is achieved, and then more H_2O_2 is added. This is done to correlate the concentration to the expected current. During flow studies this is used to be able to measure how much concentration is reacting at the electrode based on the detected current. Chronoamperometry is beneficial because it can be incorporated as an in-line detection method, giving real-time measurements.

Multiple chronoamperometry studies were conducted, however, currents obtained were randomly noisy and did not show distinguishable peaks due to the added concentrations. The red arrows in Figure 11 indicate when H_2O_2 was added to the working volume. Instead, there was a slow and steady increase in current, with no steady state between additions as seen in Figure 11.

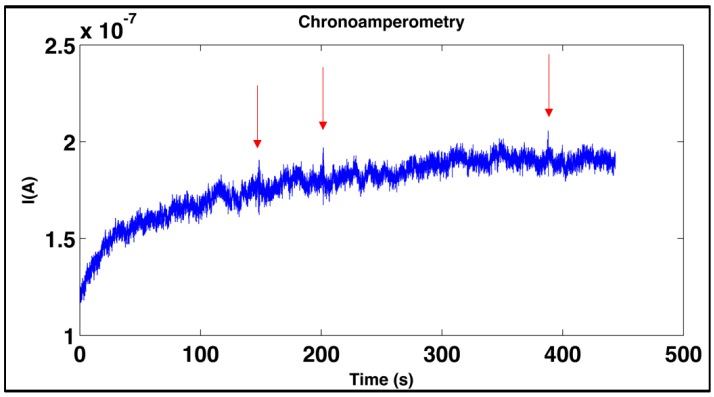

Figure 11: Chronoamperometry study.

The lack of distinguishable steps in current due to the H_2O_2 additions are possibly due to the diffusion layer thickness. The thickness of the diffusion layer is inversely proportional to the current and can build up on the electrode, causing noise in the signal [29]. One possible solution is to introduce a uniform mixing system such as a magnetic stir bar, fluid pump system, etc. However, any mixing system would interfere with the natural diffusion of H_2O_2 and results would be irrelevant to the flow study. A second solution is to alter the working electrode to avoid diffusion layer build up. Experiments were continued using the CV method to maintain simplicity within the electrochemical setup and avoid the necessity to alter the working electrode.

Repeatability

Further CV experiments yielded results with lower current to concentration ratios that were less linearly correlated. Changes in scan shape and baseline flatness were also observed. A series of troubleshooting experiments were conducted in attempts to decipher and correct the reason why the increase in current per concentration was lower than previous results and the overall shape of the scan had changed. The main

hypotheses were that changes were due to polishing, degrading H_2O_2 concentration, or leaking from the reference electrode.

Repeated Chronoamperometry (RCA) was used to alternate the potential between 500 and -500 mV in an attempt to clean up surface oxidation that could lead to a loss of signal. The initial baseline scan was high but the overall shape was much closer to the expected shape. Once the RCA was complete and the overall shape in scans returned to expected, the reference electrode and stock concentration were checked.

The reference electrode was switched to a new leak free style to determine if there were problems with the reference electrode. The baseline changed slightly due to the new reference electrode, but the shape remained the same, as seen in Figure 12 (LF RE).

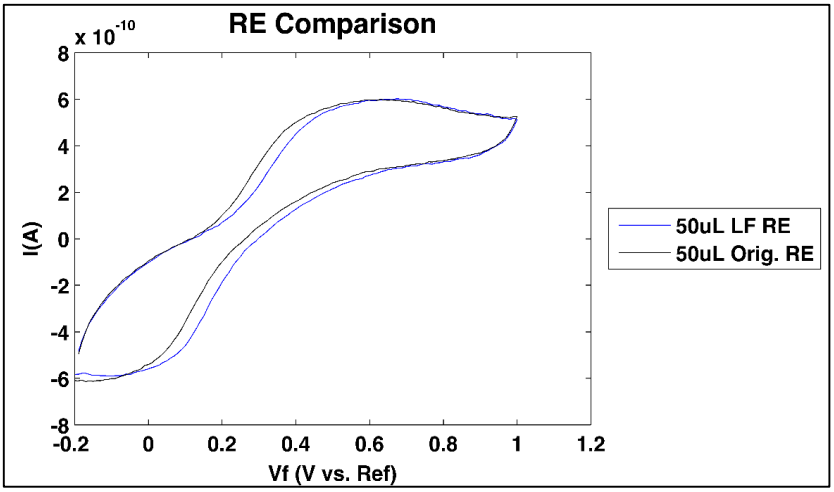

Figure 12: CV scans using a leak-free RE and the original RE.

To check whether the stock H_2O_2 had degraded, a fresh sample of H_2O_2 (3 %) was diluted to the same molarity as the solutions using 30%. Additions of concentrations alternated between the two solutions to see if the original stock solution may have degraded. Figure 13 shows the currents obtained at 610 mV. Data from the 3% H_2O_2 is circled in red. Currents from both types increased with concentration at the same rate, implying that the original stock solution had not degraded.

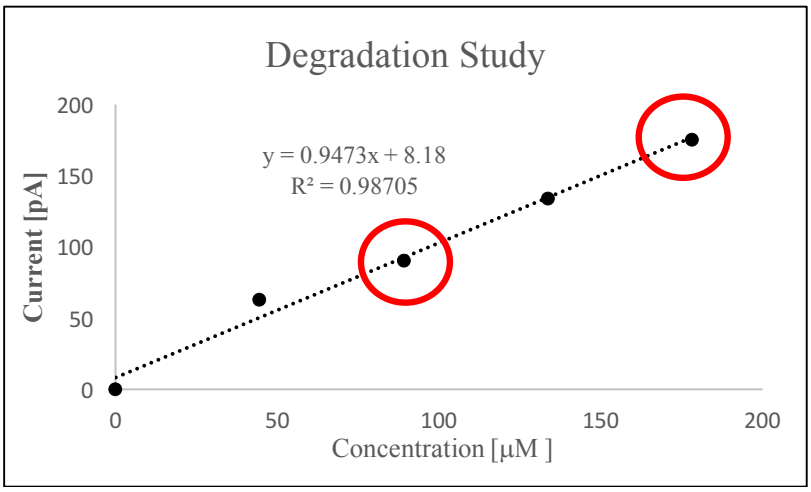

Figure 13: Degradation study of stock H_2O_2.

Over time the CV scans were showing irregularities including random results, peaks not as pronounced, baseline and overall shape changes, and less correlated trendlines of current to concentration. As a result, the detection method was switched to colorimetry to improve repeatability and simplify the data collection process.

3.2.2 Colorimetry

Setup

A peroxidase activity assay kit was used as an alternate detection method. The kit consists of assay buffer, a fluorescent peroxidase substrate suspended in dimethyl sulfoxide (DMSO), and horseradish peroxidase (HRP). Typically, the kit is used to detect peroxidase activity within a biological system, by catalyzing a reaction between H_2O_2 and peroxidase enzymes occurring in the system. The reaction creates a colorimetric product proportional to the amount of peroxidase activity.

For these studies, the standard curve procedure of the kit was used to create a linear relationship between a controlled amount of HRP and known amounts of H_2O_2 (in nanomole). From this relationship, samples can be quantified to indicate how many nanomole of H_2O_2 each one contains which can then be related back to the concentration of the samples and indicate the local concentration. The range of the standard curve is 1-5 nmol H_2O_2 per sample.

A BioTek Epoch plate reader (Figure 14) with Gen5 software was used to obtain absorbance measurements at 570 nm. A standard curve (outlined in the calibration section) was created to determine the linear relationship between the amount of H_2O_2 present and measured absorbance.

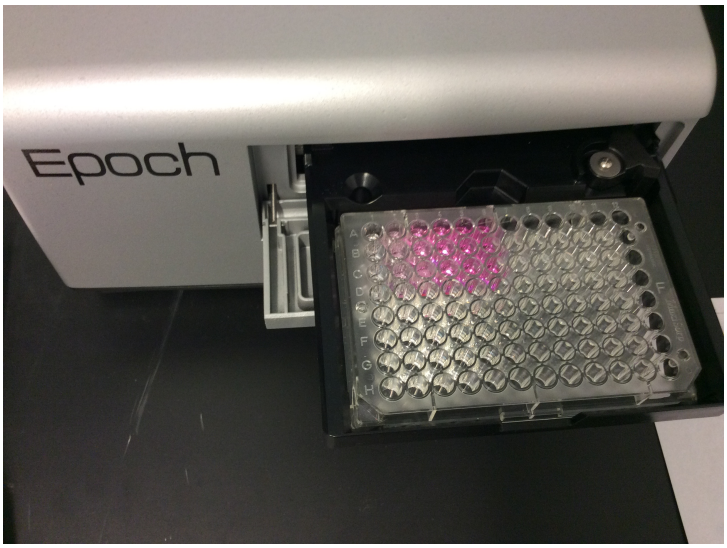

Figure 14: Epoch plate reader used in colorimetric setup.

Calibration

The standard curve procedure uses a set amount of fluorescent peroxidase substrate (2 µL), and HRP (48 µL) per plate well. Each well contained 0 (blank), 1, 2, 3, 4 or 5 nmol H_2O_2.The wells were topped off with PBS in order to bring each well volume up to 100 µL. Triplicates of each amount were used during each reading, and the measurements were averaged. Data obtained from each scan was constructed into an Absorbance vs. H_2O_2 plot. The slope of this plot (which should be linear) was used to indicate how much absorbance increased per nanomole of H_2O_2. The slope was interpolated to decipher the unknown concentration of extracted samples.

The initial standard curve was obtained using the protocol for the Peroxidase Activtity Assay kit (Sigma Aldrich MAK092), described above. The baseline absorbance was subtracted from all data and was plotted as Absorbance vs. H_2O_2 (Figure 15). The curve showed a linear relationship between absorbance and H_2O_2 (Absorbance=0.1303* nanomole H_2O_2, R^2=0.96358). A follow up curve returned similar results.

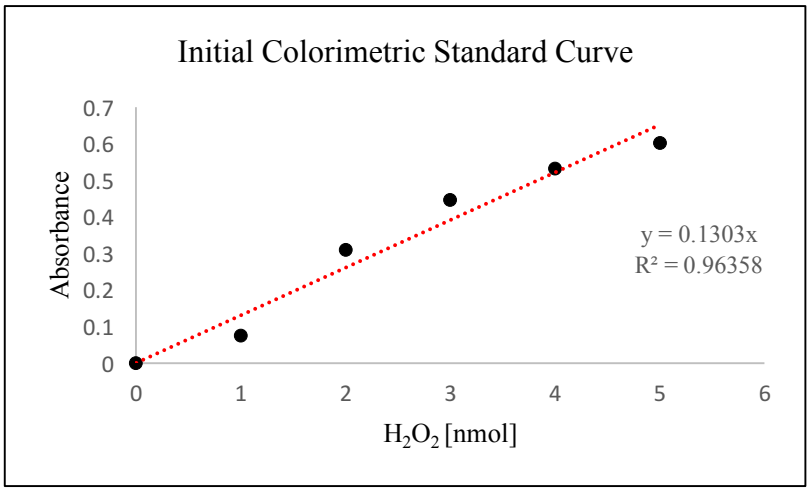

Figure 15: Standard curve obtained using Peroxidase Activity Assay kit.

A third standard curve was created based on a lower level of HRP per well (~.56 µL) to see if it was possible to decrease the amount used per run. The assay buffer was also switched to PBS in order to decrease the bubbles present. Results gave a slightly higher slope of y=0.1427x with a better correlation, R^2=0.99616. These results indicate that it is possible to conserve HRP by using a lower level and that PBS can be substituted in to rid the samples of bubbles that may obscure readings.

Ampliflu Red

An alternate approach utilized Ampliflu Red suspended in DMSO, as the fluorescent peroxidase substrate. Ampliflu Red (5 mg) was mixed with 5 mL DMSO to obtain a 3.88 mM solution. Approximately 1.67 µL per well was used, which included a slight factor of safety from the calculated minimum required.

A standard curve was created using the Ampliflu Red (AR) solution as the new fluorescent peroxidase substrate. For 18 wells, a master reactor (MR) mix of 10 µL HRP, 30 µL AR, and 920 µL PBS was prepared and divided into the 18 wells, along with H_2O_2 and PBS according to the standard curve directions. The data was then read at 571 nm (per AR instructions), corrected from baseline, and plotted into an absorbance vs H_2O_2 plot. Three standard curves were averaged to find the rate of increase (Figure 16).

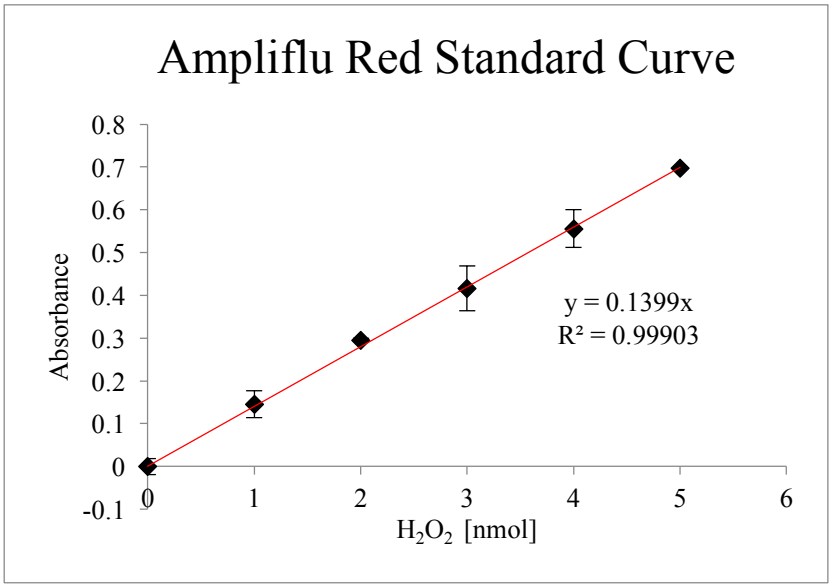

Figure 16: Averaged standard curve using Ampliflu Red.

Another standard curve was created to test the detection limits prescribed by the test kit. This calibration used the averaged data from samples containing 0, 1, 2, 3, 4, 5, 6, 7, or 8 nmol H_2O_2. At levels > 5 nmol, results were no longer correlated to the linear trend observed from 1-5 nmol. This indicated that the reliable range of was from 1-5 nmol (Figure 17).

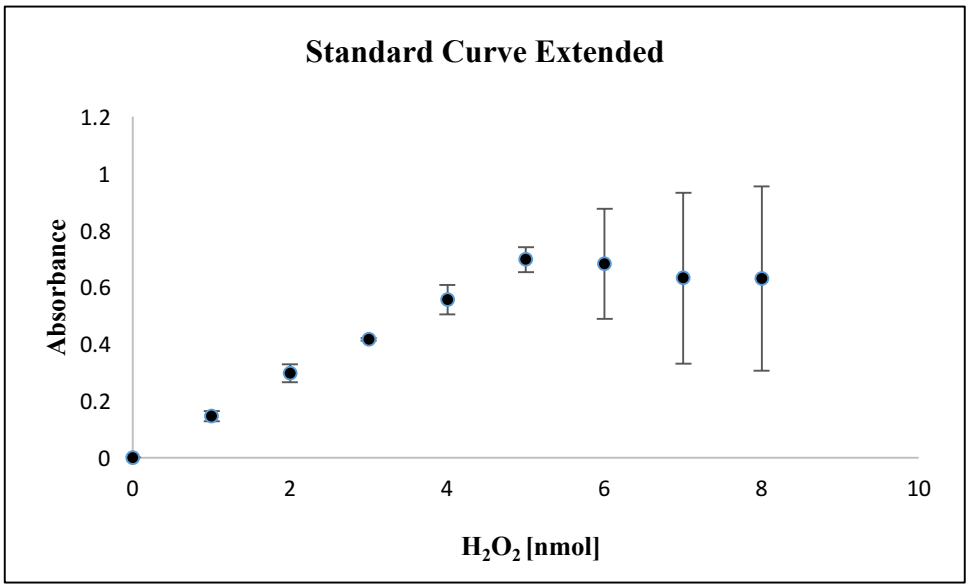

Figure 17: Extended standard curve using Ampliflu Red.

4.0 Experimental Testing

4.1 Method

For each experiment, the same microfluidic device was used. The device was first filled with 100 µL PBS which settled for approximately 2 minutes. H_2O_2 (0.5 µL of 8.8M) was pipetted into the inlet and allowed to diffuse through the device. Samples (0.5 µL) were extracted from the reservoir and deposited into separate wells of a glass plate containing 150 µL PBS each. After all samples were collected, 150 µL of a master reactor mixture was injected into each well. The master reactor contained 920 µL PBS, 30 µL Ampliflu Red (AR), and 10 µL horseradish peroxidase (HRP). The wells containing the sample, PBS, and master reactor incubated for 5 minutes and were then each divided into three separate wells on a plastic plate-reader plate. The separation process allowed for samples to be run in duplicate and a greater amount of sample to be run but still remain in the range of the standard curve (1-5 nmole). The holding containers also decreased the chance of losing any amount of such small sample volumes during transfer. Each plate was scanned using at 570 nm in a BioTek Epoch plate reader. Absorbance data was obtained through Gen5 software, corrected, and then related to the calibrated standard curve to decipher the amount of H_2O_2 in each extracted sample. The extraction was video recorded and time stamps associated with each extraction were obtained. An illustration of the experimental setup is found in Figure 18.

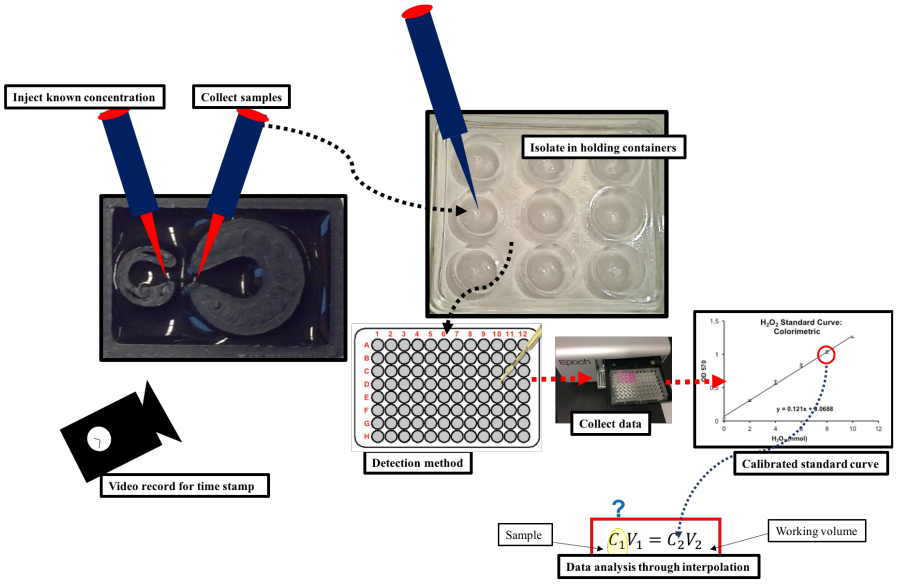

Figure 18: Experimental setup for sample collection, detection, and analysis.

The range of the kit was 1-5 nmol so dilution factors were used to maintain each sample within the range. To improve the resolution of the initial samples (0-20 seconds) the first two samples (~5 seconds and ~10 seconds) were deposited into wells containing only 50 μL PBS and 50 μL master reactor was introduced. These samples were then transferred as only one sample into the plate reader plate. This is considered a dilution factor of 1X. To ensure that the sample was not greater than the standard curve limit, the later samples (starting at ~25 seconds) were deposited into wells containing 300 μL or 500 μL PBS. From each well, three samples of 50 μL were transferred into the plate reader plate. The master reactor (50 μL per well) was then added. The intensity data was correlated to the standard curve and then a dilution factor of 6X or 10X was applied in order to calculate the number of nanomole of H_2O_2 in each 0.5 μL sample taken from the device.

The final set of experiments began the sampling process at approximately one minute after the H_2O_2 was introduced to better examine steady state diffusion. The last two samples from these experiments were extracted from the side of the channel, and the channel itself as a way to validate that the concentrations were at unity with each other. All samples were deposited into 1000 μL PBS and a dilution factor of 20X was applied.

4.2 Data analysis

Data analysis focused on quantifying the transient diffusion towards the "DA neuron" by examining the amount of H_2O_2 (nmol) per 0.5 μL sample had reached this area. A comparison was made to the number of nanomole sampled at the side of the channel. Although the concentrations throughout the device never fully equalized within the timeframe of the experiments, there appeared to be a localized equilibrium indicated by a plateau in the data. To validate this pseudo-equilibrium, single samples from the channel and side were taken at the end of several experiments. Data from these samples were compared to those from the reservoir at the localized equilibrium. Video was also used to help visualize the real time diffusion of H_2O_2, which was pipetted directly into a device containing the Ampliflu Red master reactor mix.

Each sample was run in triplicates, with the exception of very early samples which were tested in single samples because of the 1X dilution factor. Samples run in triplicate were averaged to obtain absorbance

data. Baseline samples extracted from the device at the beginning of each experiment, were also scanned and averaged. The baseline was subtracted from each sample average. Final data was converted into nanomole H_2O_2 by dividing the averaged absorbance data by the standard curve slope of 0.1399 (absorbance/nmol). Dilution factors of 1X, 3X, 6X, 10X or 20X were applied to obtain the number of nanomole present in each extracted 0.5 μL sample.

The data from the side and reservoir was examined for results which were not within the range of the kit. Data points < 0.88 nmol and > 5 nmol were removed and the remaining were averaged by 10 second bins. The data from the channel and side (taken at the end of experiments) were also averaged and standard deviations were used to obtain ranges of each during the localized equilibrium.

To examine whether the means of each location were significantly different during equilibrium, an analysis of variance (ANOVA) was performed comparing the side, channel and reservoir data. ANOVA is a method of test variance amongst two or more sets of data. The premise is to assume a null hypothesis that the data is not significantly different. The ANOVA calculates the probability that the null hypothesis is true based on averages and standard deviations. It is standard practice to use $p < 0.1$ or $p < 0.05$ to reject the null hypothesis. In this case, a high p-value would help to reinforce whether the data can be considered at equilibrium by validating that the averages of each do not differ significantly. To ensure no significant differences between individual samples, follow up analysis was conducted using a Tukey test as well as Scheffe and Bonferroni & Holme multiple comparisons.

4.3 Results:

4.3.1 Transient analysis of H_2O_2 transport

Reservoir sample data was compiled from a total of 21 experiments. Each set of data was examined and outliers were removed. The data from all experiments was then averaged into 10 second bins. Averaging the data into bins helped to filter any offsets that may have been due to changes between experimentation (i.e. injection differences). The averages, shown in Figure 19, were then plotted versus time in 10 second increments. In Figure 19, error bars represent the standard deviations from the mean.

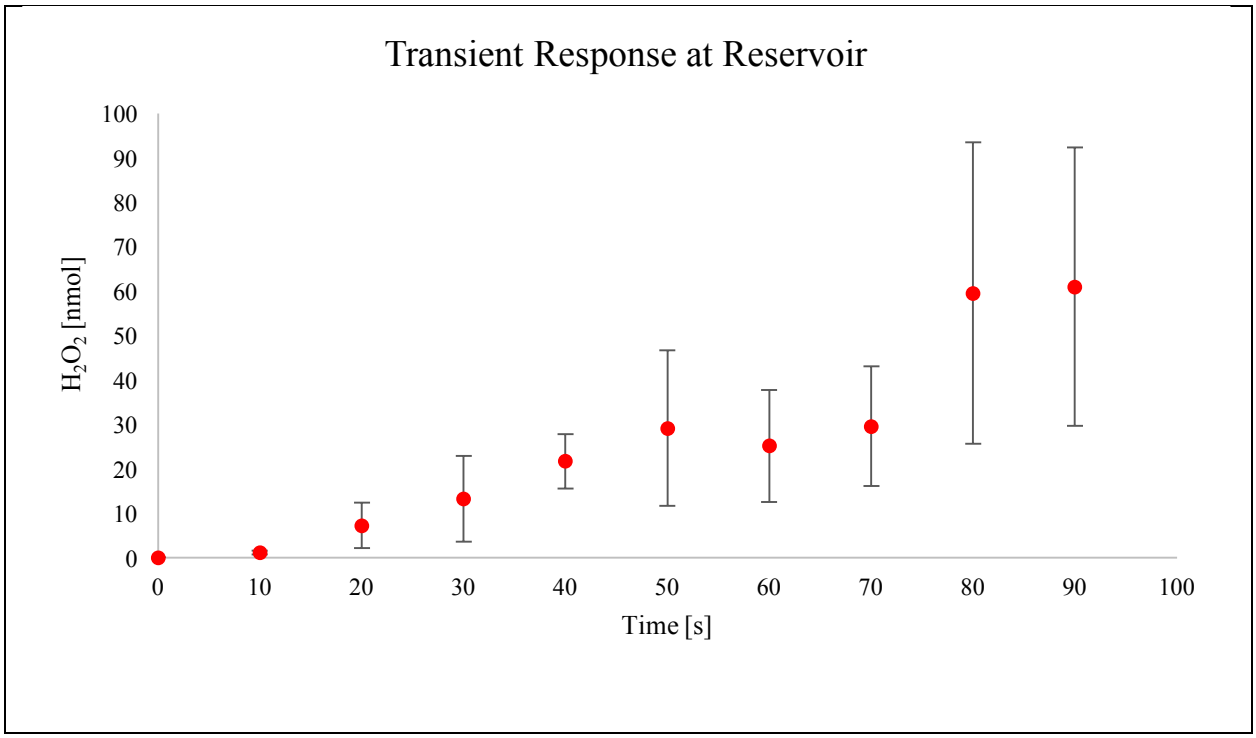

Figure 19:Reservoir data, averaged into 10 second bins.

Side sample data was compiled from a total of 11 experiments. Each set of data was examined and outliers were removed. The data was then averaged into 10 second bins and plotted with the reservoir data in 10 second increments (Figure 20). The reservoir data is shown in red and the side data is shown in navy. Error bars were applied using the standard deviations from each bin.

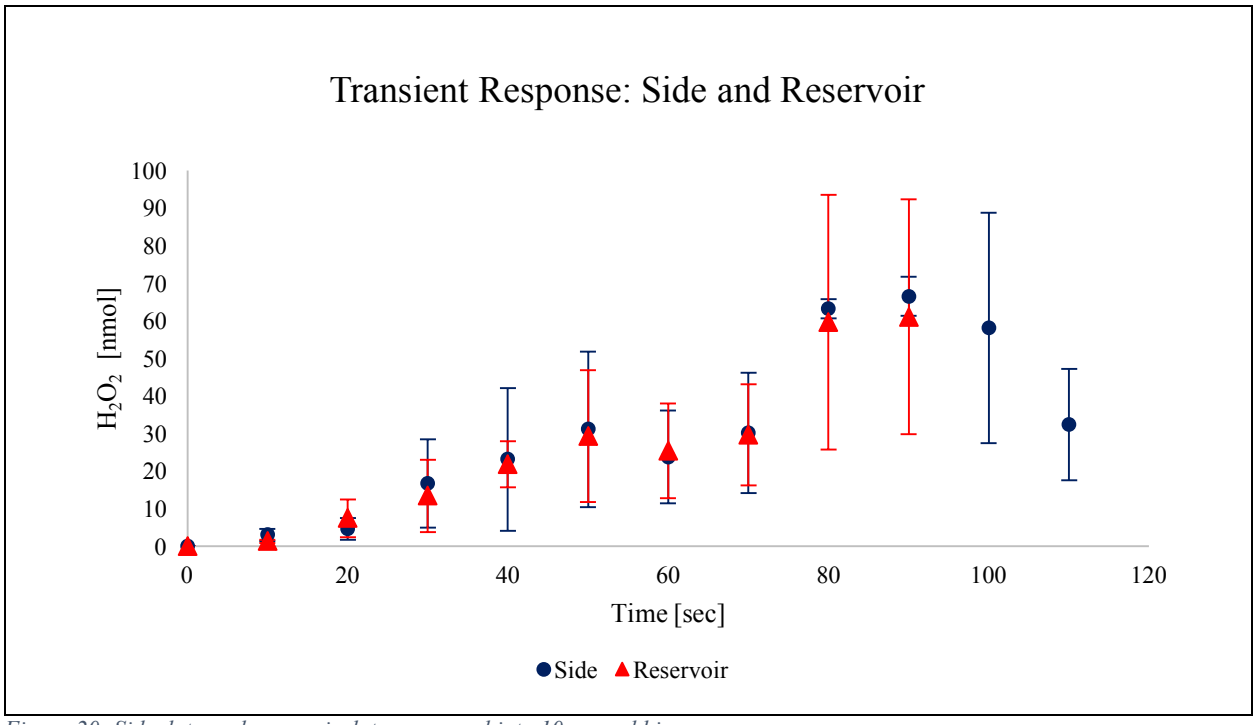

Figure 20: Side data and reservoir data, averaged into 10 second bins.

The rate of increase in H_2O_2 per sample for the reservoir and side is initially ~0.123 nmol/s and ~0.291 nmol/s respectively. There seems to be a curvilinear trend for the data up until the 50 second bin for both the side and the reservoir. The region between 50-80 seconds was most likely out of range with an incorrect dilution factor applied. There is evidence of a plateau of ~60 nmol (reservoir) and ~63 nmol (side) beginning at 80 seconds. The side data shows a decrease after 90 seconds. Error bars are varied as time progresses. Although the reservoir data shows high error bars around the plateau, the error bars for the side data are minimal (2.5 and 5.2 nmol).

Experiments collecting side data were conducted after the reservoir data had been collected. During these experiments, the dilution factors were more finely adjusted, leading to less error. Statistical analysis was used to examine the validity of a plateau occurring at 80 seconds and takes into account the standard deviations on all data analyzed. This is explained further in section 4.3.3.

4.3.2 Concentration Conversions and Percentage

The measured amount of H_2O_2 was converted to concentration using Equation 2, interpolating for concentration. The volume of each sample was 0.5 µL, and the obtained concentration was assumed to be the local concentration at the extracted time. The percent totals were calculated using Equation 3, where the original concentration was 8.8 M.

$$nmol = Concentration * Volume \quad [2]$$

$$\% \, Total = \frac{Concentration}{Original \, Concentration} \times 100 \, \% \quad [3]$$

The amount of H_2O_2 in terms of nanomoles, concentration, and percent of the original amount are found in Table 3.

Table 3: Concentration and percent total for reservoir and side.

	Concentration					
	Reservoir			Side		
Time [s]	Amount [nmol]	Conc. [mM]	% Total	Amount [nmol]	Conc. [mM]	% Total
0	0	0	0.00	0	0	0.00
10	1.23	2.46	0.03	2.91	5.82	0.07
20	7.34	14.68	0.17	4.49	8.97	0.10
30	13.35	26.71	0.30	16.55	33.11	0.38
40	21.78	43.56	0.49	23.04	46.09	0.52
50	29.20	58.40	0.66	31.03	62.06	0.71
60	25.23	50.46	0.57	23.69	47.37	0.54
70	29.63	59.25	0.67	30.06	60.12	0.68
80	59.58	119.16	1.35	63.11	126.23	1.43
90	61.01	122.01	1.39	66.43	132.87	1.51
100				58.09	116.17	1.32
110				32.31	64.61	0.73

During the localized equilibrium, the averaged concentration at the reservoir plateaued between 119.16 and 122.01 mM, which is 1.35-1.39% of the concentration in the original 0.5 µL sample. The averaged concentration of the side during the same period was measured to be slightly higher (126.23-132.87 mM) which was 1.43-1.51% of the original concentration. The disparity in original and final concentrations is due to the H_2O_2, initially very dense in a 0.5 µL sample, diffusing outward to a volume estimated to be approximately 34.22 µL (through observation of the visual study).

These values can also be considered in terms of the absolute amount of H_2O_2 (nanomole). The original amount of H_2O_2 was 4400 nmol. With the estimated volume and considering the amount of H_2O_2 in the reservoir (61 nmol), the total amount within the volume would be ~4174.84 nmol (Equation 4), a 5.1% difference. This is most likely attributed to the fact that the volume was not a control volume and H_2O_2 continued to exit out of the sides, while the central area reached a localized equilibrium.

$$\frac{Total\ H_2O_2}{Total\ Volume} = \frac{Local\ H_2O_2}{Sample\ Volume} \quad [4]$$

The information found in Table 3 may be taken into account in experimentation, especially when the H_2O_2 is exogenously applied to neurons.

4.3.3 Localized equilibrium

Although the device never fully normalized within the timeframe of the experiments, there appeared to be a localized equilibrium indicated by a plateau in the data. To validate this equilibrium, single samples from the channel and side were taken at the end of several experiments. Data from these samples were compared to those from the reservoir at the localized equilibrium. Figure 20 shows the averaged data from reservoir, channel, and side during the plateau, at 60, 68, and 63 nmol, respectively. Standard deviations were 33.9, 33.5, and 2.6 nmol, respectively, and are shown as red and black bars.

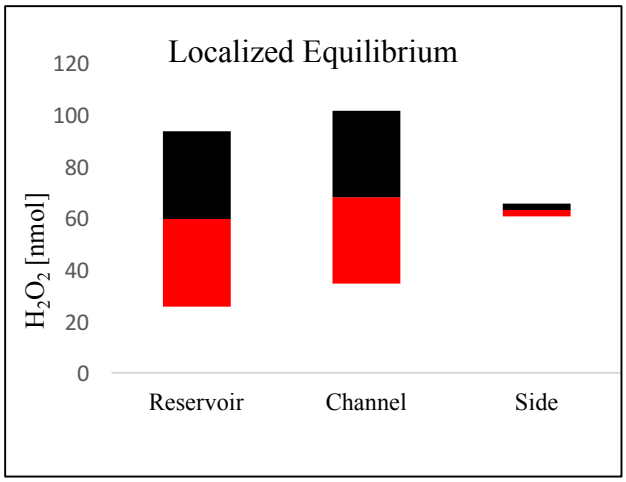

Figure 21:Localized equilibrium data from the reservoir, channel, and side.

An analysis of variance (ANOVA) was performed that compared the side, channel and reservoir data. The test returned a probability value of p= 0.9146, indicating that there were no significant differences between the amounts of H_2O_2 at each location. To ensure no significant differences between individual samples, follow up analysis was conducted using a Tukey, Scheffe and Bonferroni & Holme multiple comparisons. As shown in Table 5, p-values indicated that there were no significant differences between any individual groups. The statistical analyses help validate that a localized equilibrium occurred around 80 seconds.

Table 4: Follow up statistical comparisons.

	Tukey	Scheffe	Bonferroni	Holm
Side vs Reservoir	0.900	0.987	2.624	0.875
Side vs Channel	0.900	0.915	2.044	2.044
Reservoir vs Channel	0.900	0.977	2.498	1.665

4.3.4 Curve fitting

By inspection, data for the amount of H_2O_2 in each sample (N_d) was fit to curves using Equation 5. This is a solution for the response to a step input, commonly used in controls engineering. The physical interpretation can be found in the discussion section.

$$N_d = A \sin \beta t \, (1 - e^{-\beta t}) \qquad [5]$$

Initially, β was obtained experimentally from $\ln\left(\frac{A-N_d}{A}\right) = \beta t$ using a semilog plot versus time, where **A** was the amount of H_2O_2 in the channel (68 nmol) during the plateau and N_d was data collected from the reservoir. Two additional **A** values were obtained by interpolating Equation 5 using data from the side and reservoir during plateau and the calculated β value (0.02) (Equation 6). The obtained values and corresponding data are listed in Table 5.

$$\frac{N_d}{\sin(\beta t)(1-e^{-\beta t})} = A \qquad [6]$$

Table 5: Coefficients for Assumed Solutions:

A [nmol]	β	N_d [nmol]	Time [s]
75	0.02	60 (reservoir)	80
81	0.02	66 (side)	90
68	0.02	Obtained using $\ln\left(\frac{A-N_d}{A}\right) = \beta t$	

Data was fit using three solutions with β= 0.02 and the corresponding **A** values. Results are shown in Figure 22 (Red = reservoir data, Navy = side data).

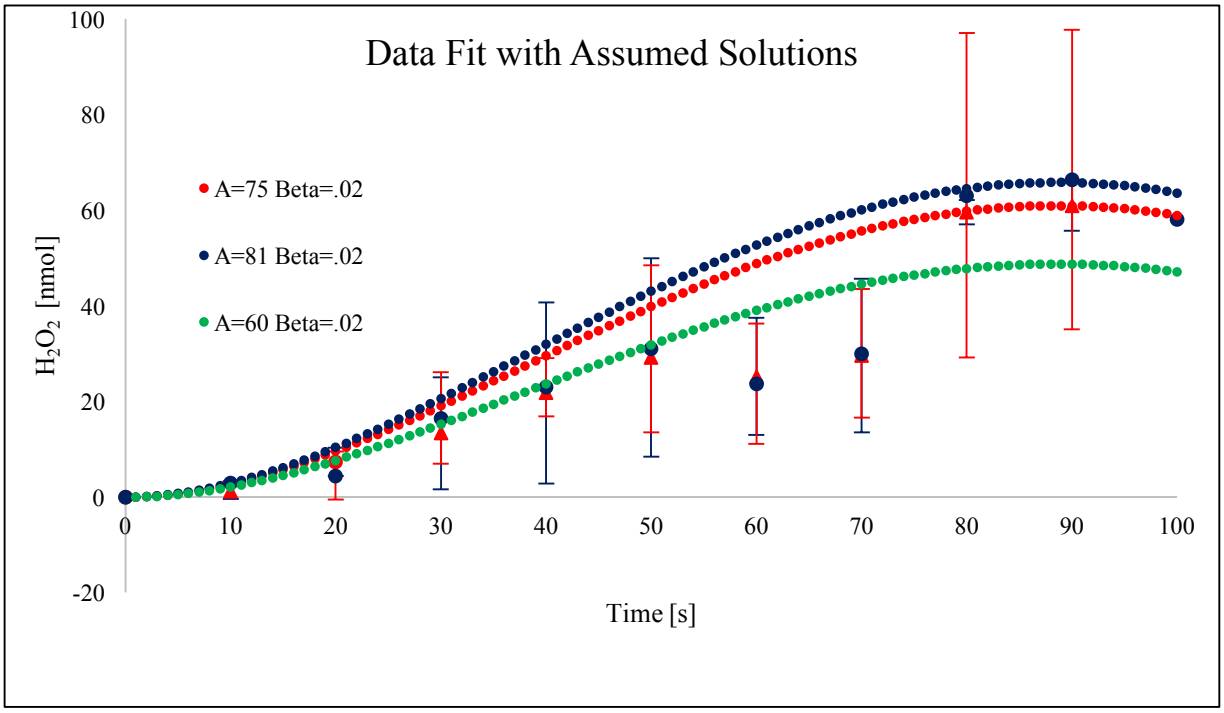

Figure 22: Side and reservoir data fit using assumed solutions

The solution using the initial β and A values follows the same trend as the early stage of the experiments (< 50 s). However, the final amplitude is not sufficient during the later stage (> 50 s), nor does it correspond to the experimental amplitudes observed during the plateau. Two more solutions were found using the corresponding data at the time of each plateau. These solutions correlate well with the side and reservoir data during the plateaus. The differences in **A** values will be examined in the discussion section. Most values of all three solutions fall within the range of the error bars for both the side and reservoir data.

The governing diffusion equation is a partial differential equation (PDE), Equation 3.

$$\frac{1}{D}\frac{\partial C}{\partial t} = \frac{\partial^2 C}{\partial x^2} + \frac{\partial^2 C}{\partial y^2} + \frac{\partial^2 C}{\partial z^2} \quad [3]$$

Where D is the diffusion coefficient and ∂C is the change in concentration. To solve the PDE, it can be separated into ordinary differential equations (ODE). Separate spatial and time solutions are assumed (Equation 4 and 5, respectively) and eigenvalue problems are used to determine the coefficients.

$$X(x) = Acos(kx) + Bsin(kx) \quad [4]$$

$$T(t) = Fe^{-k^2Dt} \quad [5]$$

The solution of each is multiplied together to obtain a transient solution in one direction (Equation 6).

$$C(x,t) = A_1 \cos(kx)\, e^{-k^2Dt} + A_2 \sin(kx) e^{-k^2Dt} \quad [6]$$

Where A_1 and A_2 are combinations of F, A, and B.

Based on the 1-D solution, it seems reasonable to fit the data with Equation 1, which is an approximation using a decaying sinusoid and is the solution to a second order ODE. To validate this assumption, data was also fit using a simplified version of the 1D diffusion equation solution (Equation 7).

$$\frac{N_d(x,t)}{A} = 1 - [\cos(\beta x) + \sin(\beta x)]\, e^{-\beta t} \quad [7]$$

Coefficients A_1 and A_2 were assumed to be the amount found in the channel during plateau (68 nmol) and previously obtained β value (0.02) was used in lieu of eigenvalues and the diffusion coefficient. All data was normalized and the curve fit can be seen in Figure 23.

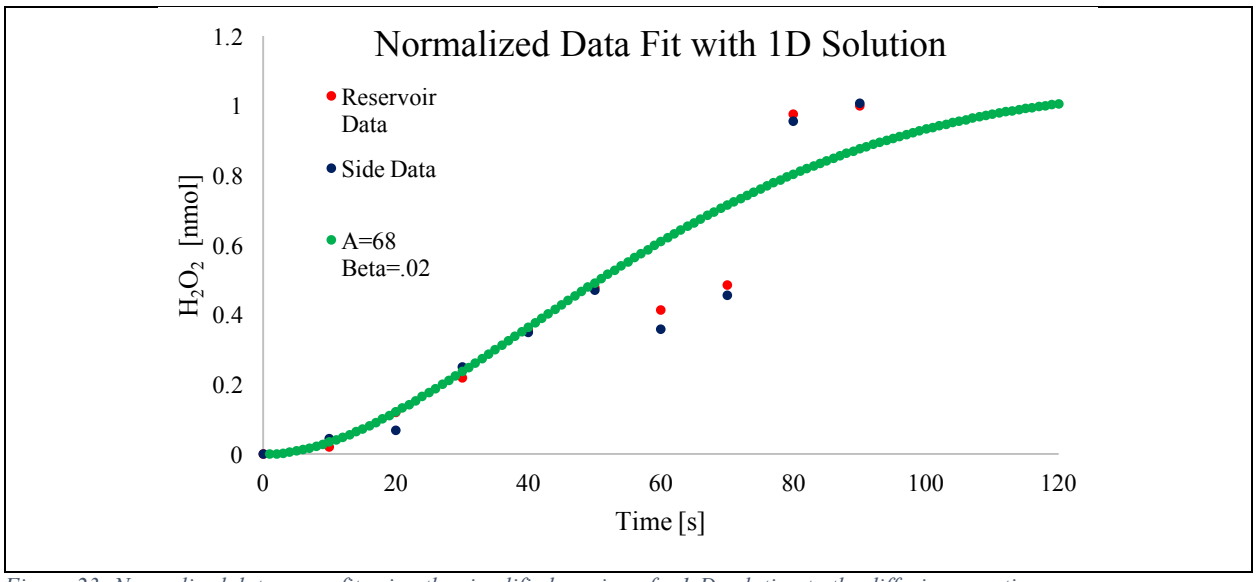

Figure 23: Normalized data curve fit using the simplified version of a 1-D solution to the diffusion equation.

The normalized data from both the side and the reservoir follow the 1-D approximation very closely until 50 seconds. After the period where the data is irregular (60-70 seconds), the experimental data is much higher than the curve fit. According to the curve, unity doesn't occur until 120 seconds, which is much later than the perceived plateau at 80 seconds. This variation could be attributed to other dynamics occurring within the device. For example, there may be a bottlenecking effect occurring at 80 seconds, leading to a quicker than predicted local equilibrium. Although the data and the curve fit differ in terms of steady state, the statistical analysis helps to validate the plateau effect at 80 seconds. It is also important to remember that the solution obtained for the curve fit was a simplification of the actual diffusion equation, leading to an approximation of what the equation might actually be. It can be assumed that the actual solution to describe the transport is a combination of the two equations used. Further mathematical modelling could be used to obtain a more accurate description.

4.3.5 Visualization

A video was recorded to help visualize the real time diffusion of H_2O_2. For the video, H_2O_2 was pipetted into a device containing the Ampliflu Red master reactor mix. The device used was not the same as the one used during experiments, it was switched to a white device which helped for visual reasons. Still images from the video are shown in Figure 23. The images were taken at 10, 40, 60, and 80 seconds.

Figure 24: Still images of real-time diffusion study at 10, 40, 60 and 80 seconds (left to right).

The initial affinity towards the sides is observed, and seen most clearly at 10 seconds. This can help validate the accuracy of the data which showed an initial increase for the side to be ~2.4 X that of the increase seen in the reservoir. The images also show that the later diffusion seems to occur outward equally in all directions, until reaching the device walls, where it is hindered (~60 seconds). At 80 seconds there seems to be a localized equilibrium between the inlet, channel, reservoir and sides. Although the device is never fully normalized, this is the region of most interest for the MSN-DA pathway. Limitations due to device geometry will be discussed further in the discussion section.

5.0 Conclusions

This study aimed to develop an experimental setup to help examine and quantify the transport within a laboratory setting. The setup focused on using an effective method to detect H_2O_2 within a flow device modeled around the geometry of the MSN-DA neuron pathway.

The experimental setup used in this research was developed around a sensitive, cost-effective, reliable, solution for detecting H_2O_2. The device was fabricated using 3-D printing, a rapid and cost effective solution. The system was calibrated and adjusted to obtain an appropriate detection signal within the range of the detection method. Sample collection and analysis was fine-tuned so that a time-dependent analysis of H_2O_2 transport was possible within the limitations of the system.

This work represents a proof-of-concept scenario and information gained here can be used for future experiments aimed at predicting H_2O_2 transport within the MSN-DA pathway.

5.1 Simulation of H_2O_2 Transport in the MSN-DA Pathway

The device was designed based on the geometry of MSN-DA pathway. Geometric features, such as the distance between the MSN and DA neurons, neuron diameter, and the diameter of neuron inlets, were taken into account for the design.

Devices were developed using polystyrene, PDMS, and 3-D printing. Due to accessibility and ease of use, the device was redesigned to be 3-D printed as an open device which allowed for easier sampling, the ability to clean and reuse, and collect samples throughout the device. The tear-shaped reservoir was a successful solution to maintain structural integrity needed during the 3-D printing process and allowed for dimensions to be created smaller than geometry with constant inner diameters.

It was necessary to amplify the actual geometry and dimensions due to fabrication constraints and exact ratios were unable to be maintained. For example, the reservoir opening to channel width ratio was 2:3 for the final fabricated device. In actuality, the reservoir opening would be about two orders of magnitude small than the channel between the two neurons (~0.05 : 3). The depth of the device was also out of proportion. The height was limited to 1.5 mm, whereas in vivo, the z-direction of the neuron could be assumed to be infinitely long compared to the channel width, which would more closely resemble spherical transport.

Both of these modifications lead to an overestimate of the actual amount of H_2O_2 reaching the DA-neuron. The larger channel width may curtail some of these effects due to a larger distance the H_2O_2 must travel. During transport, there is more time for outward diffusion. A parametric study would lead to more insight on how these combinations affect the actual results.

5.2 Experimental Setup to Quantify H_2O_2 Transport

H_2O_2 was introduced into the device at the inlet, allowed to diffuse freely through the channel, and sampled at multiple locations throughout the device, depending on the experiment. To quantify the amount in the sample, and thus the local concentration, colorimetry was used as the detection method.

Initially, cyclic voltammetry and chronoamperometry were experimented with, however, repeatability was unsuccessful. Colorimetry offered a much simpler, more standardized approach. Unfortunately, the reliable range of quantification was limited to 1-5 nmol. Samples were diluted differently so they could be tested and remain within this range. This offered a feasible solution to extend the limits of the colorimetry kit. The dilution factors were adjusted for several time zones of the experiment. Most results were reliable and repeatable, with the exception of one zone.

5.3 Experimental Testing & Results

Both reservoir and side data follow similar trends, with the rate of diffusion to the side being slightly higher than that of the reservoir. This is what is expected because of the difference in size between the reservoir inlet and the outlet toward the side. The path of least resistance is out the side and therefore the diffusion follows that path. Initially, the rate difference was ~2.4X (.291: 0.123 [nmol/s]). The difference can be explained partially by the differences in hydraulic diameters, D_H, (4X the flow area, divided by the wetted perimeter) which are approximately 2 mm and 1.71 mm for the side and reservoir, respectively. However, the side D_H is only 1.17X that of the reservoir. Another explanation could be from the rounded edges of the "MSN" which may also decrease resistance, and allow for more transport toward the side before diffusing towards the reservoir.

The initial difference in rate does not consistently stay at ~2.4X. This could be due to the area around the rounded edges and within the side channel filling up and creating somewhat of a bottle-neck effect. The gradient in concentration is not as high and therefore the driving force of diffusion decreases. It could also be regarded as leveling the playing field between the resistances due to opening size differences seen

between the reservoir and side. Any differences due to an affinity to travel towards the side instead of the reservoir could be approximated to be two fold due to the axis of symmetry. There are two sides and only one reservoir, so the rate at which H_2O_2 is transported out the sides has twice the effect on the decreased amount allowed to travel to the reservoir.

There was a plateau observed beginning around 80 seconds for both the side and reservoir. The difference between the original amount (4400 nmol) and the calculated amount based on volume and amount of H_2O_2 in the reservoir (61 nmol), was approximately 5%. This is most likely attributed to the fact that H_2O_2 continued to exit out of the sides, while the central area reached a localized equilibrium. There could also be slight variations of concentration within the localized area.

To validate the perceived equilibrium, data from the side and channel were compared to reservoir data. Although the amounts varied slightly (68, 60 nmol for the channel and side respectively), analysis of variance (ANOVA) results indicated that there were no significant differences between data. Tukey, Scheffe and Bonferroni & Holme multiple comparisons also indicated that there were no significant differences between individual groups. Therefore, the variation between the original amount and the calculated amount is not due to statistically significant differences of concentration throughout the localized area.

Although on a molecular level diffusion is random, the mass transport can be estimated through transient analysis. The data was first fit using a common solution to a step input, used in controls engineering. The physical interpretation of the solution is that the measured amount (output) is equal to the difference between the set point (assumed input) and the effects that the system has on the set point. This is similar to a closed loop feedback control system in which the concentration gradient is the "error" or difference between achieved equilibrium and the actual amount present. When the error is zero, meaning there is no concentration gradient, the diffusion plateaus at equilibrium.

A was approximated as the amplitude seen at equilibrium. Initially, this correlates well with the data. For the later part of the transient analysis, **A** must be adjusted to be higher so that the calculated output is as high as the actual amount at plateau. The differences could be due to noise and disturbances within the system, such as bottle-necking effects due to geometry, side walls, and channel saturation. Although **A** values vary between solutions, all β values used were the same (0.02). This is a good indication that the developed solution is in close proximity of the actual solution. Also, most values of all three solutions fall within the range of the error bars for both the side and reservoir data.

Data was also fit using a simplified 1-D diffusion solution, which was highly correlated to the beginning of the transient response of both the reservoir and side normalized data. During the pseudo-equilibrium, the experimental data was higher than that of the theoretical data which predicted equilibrium at ~120 seconds. Although data and the curve fit differ in terms of steady state, the statistical analysis helps to validate the plateau effect at 80 seconds. Again, these effects may be due to uncharacterized dynamics occurring within the device due to its irregular geometry. It may also be due to an oversimplification of the actual diffusion equation. These solutions can be used to approximate the predicted transport, however, the actual solution is most likely a combination of all equations used. Further mathematical modelling could be used to obtain a more accurate description.

The video recording really helped to visualize the real time diffusion of H_2O_2. The initial affinity towards the sides is observed, which helped validate the accuracy of the differences in data between the side and reservoir. It also helps to make sense of the later diffusion, which seems to occur outward equally in all directions, and the effects that the side walls have on outward diffusion. At 80 seconds there is visual evidence of the localized equilibrium between the inlet, channel, reservoir and sides.

5.4 Future Work

The experimental setup and transient analysis performed in this work is a simplified version of the actual MSN-DA pathway. Geometry and dimensions have already been discussed as limitations to the findings. Other limitations include the lack of H_2O_2 metabolizers and diffusion barriers within the production neuron.

In the presence of peroxiredoxins, which convert H_2O_2 to H_2O with the enzyme catalase, the diffusion length of typical amounts of H_2O_2 is estimated to be extremely limited (a few fractions of a micron), based on simulations. Incorporation of metabolizers into the micro-fluidic system is an essential part of whether or not H_2O_2 can reach its targets.

Diffusion away from intracellular production sites is different from diffusion through extracellular fluid [15]. It has been shown that H_2O_2 does not diffuse freely within cytoplasm but instead forms pools or “micro-domains” and acts locally. Diffusion within the cytoplasm is estimated to only reach a few microns, which would hinder its ability to leave the production cell.

By incorporating the above mentioned elements into the device, the results would become more accurate. The overall amount of H_2O_2 that reach the reservoir is expected to be much less.

Modeling the diffusion as a closed loop control system could aid in the development of modelling the effects of H_2O_2 in the brain. The transient response observed in this research could be used as the input which would extend to the DA neuron, potentially leading to inhibitory effects. This would extend the applications of the information gained here and advance the possibility of examining such networks within the brain.

APPENDIX A

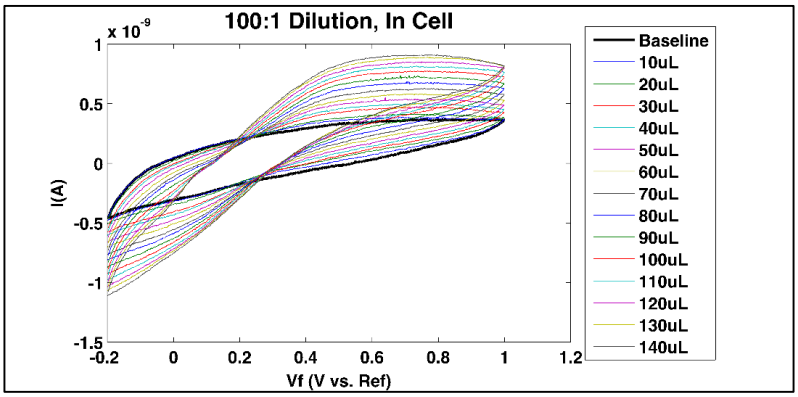

Figure 25: First attempt to replicate initial CV results showing an observed change in overall shape.

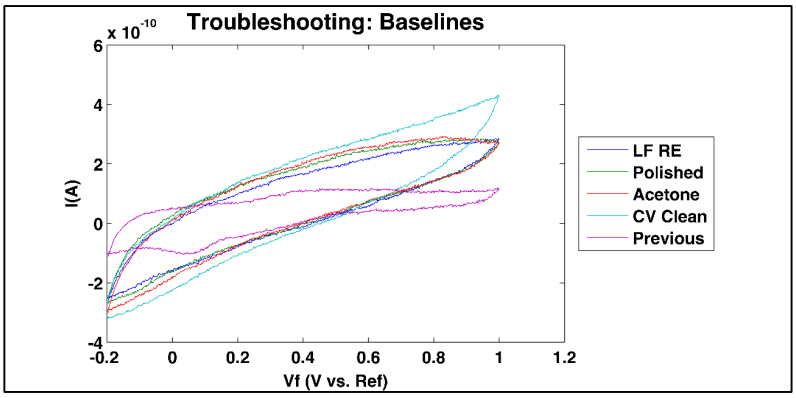

Figure 26:Comparison of baseline scans obtained during the troubleshooting process and the previously obtained baseline. No method successfully obtained a baseline similar to the initial baseline.

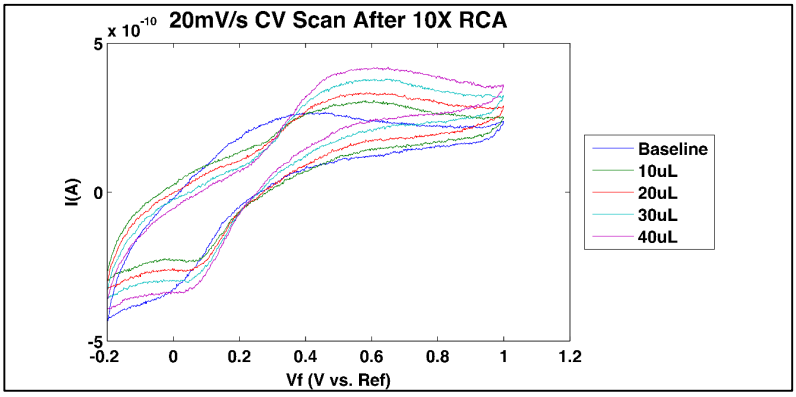

Figure 27: Comparison of CV scans obtained with 30% H_2O_2 vs. 3% H_2O_2 after 10 cycles of Repeated Chronoamperometry, using a leak-free reference electrode. The scans were set to 20mV/sec, step size=2. The 20µL and 40µL additions were from solution made with 3%, store bough H_2O_2.

APPENDIX B

A study of polystyrene was conducted to compare laser cutting, inkjet printing, and laserjet printing before shrinking. Before shrinking, it was found that the laser cutter worked well if the polystyrene was covered with tape to disperse some of the heat from the laser. The ink from the inkjet printer never dried, and the laserjet printer worked well but there were difficulties with alignment when several prints were attempted to build up the mask. After shrinking, the laser cut polystyrene deformed and created gaps in the channels, and the laser jet polystyrene also deformed but the mask did increase in height while shrinking in the width and length directions. These results are shown in Figures 28 and 29.

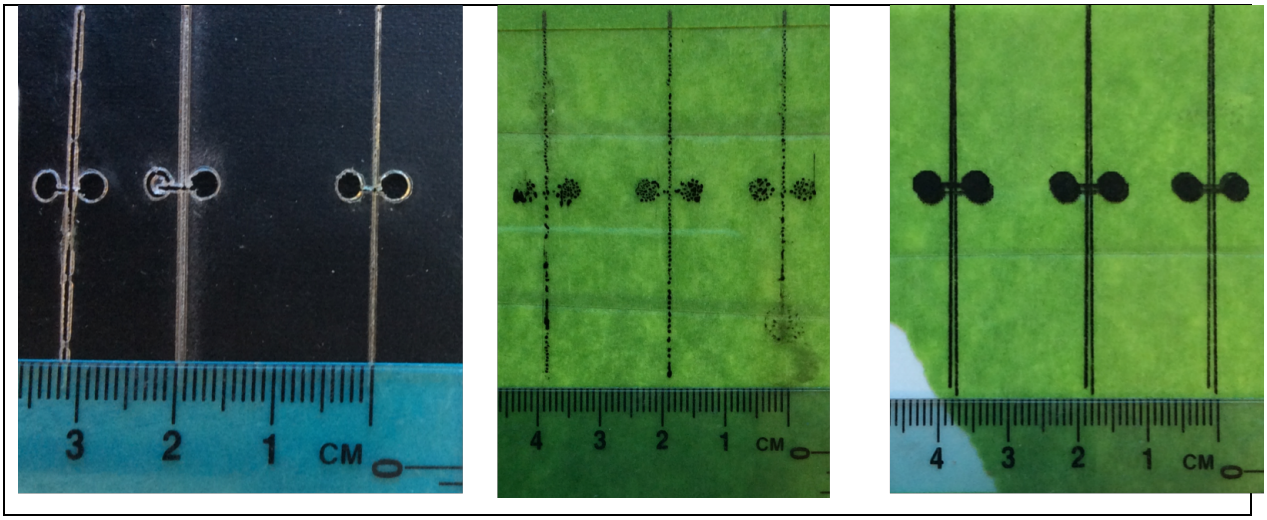

Figure 28:Polystyrene Shrinky Dink study (left to right: laser cut, inkjet printing, and laserjet printing)

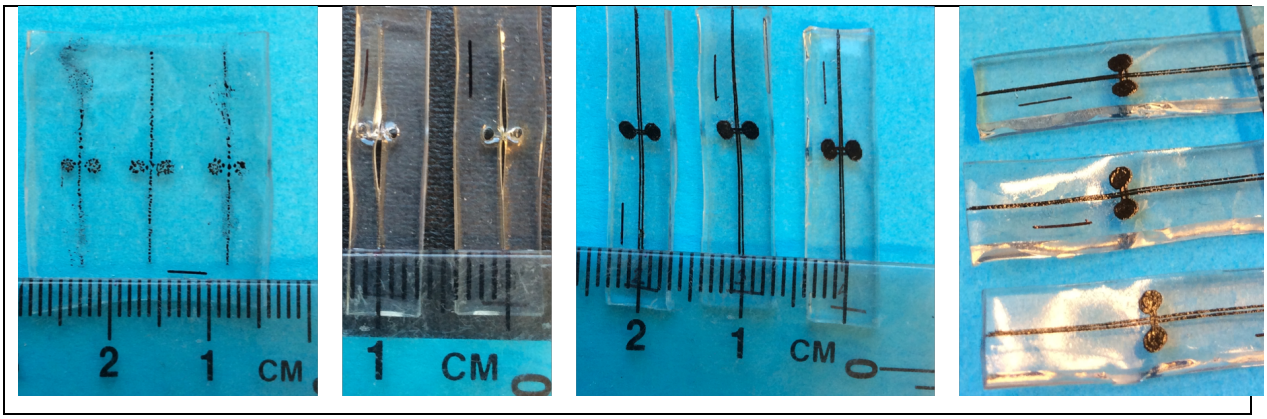

Figure 29: Polystyrene Shrinky Dink study, post heat treatment: dimensions and warpage (left to right: inkjet, laser cut, laserjet printing, laserjet printing)

6.0 REFERENCES

[1] N. D. Volkow, J. S. Fowler, G. J. Wang, and J. M. Swanson, "Dopamine in drug abuse and addiction: results from imaging studies and treatment implications," *Molecular Psychiatry,* vol. 9, no. 6, pp. 557-569, 2004.

[2] H. S. Jeong and Y. A. Chung, "Contribution of neuroimaging in the diagnosis of brain disorders: Recent findings and future applications," *International Journal of Imaging Systems and Technology,* vol. 26, no. 2, pp. 124-135, 2016.

[3] I. H. C. H. M. Philippens, B. A. 't Hart, and G. Torres, "The MPTP marmoset model of Parkinsonism: a multi-purpose non-human primate model for neurodegenerative diseases," *Drug Discovery Today,* vol. 15, no. 23, pp. 985-990, 2010.

[4] P. M. Grasby *et al.*, "Evidence for striatal dopamine release during a video game," *Nature,* vol. 393, no. 6682, pp. 266-268, 1998.

[5] H. F. Hou *et al.*, "Reduced Striatal Dopamine Transporters in People with Internet Addiction Disorder," *Journal of Biomedicine and Biotechnology,* vol. 2012, pp. 1-5, 2012.

[6] S. H. Kim, S. H. Baik, C. S. Park, S. J. Kim, S. W. Choi, and S. E. Kim, "Reduced striatal dopamine D2 receptors in people with Internet addiction," *Neuroreport,* vol. 22, no. 8, pp. 407-411, 2011.

[7] H. C. Guo *et al.*, "Two-photon fluorescence imaging of intracellular hydrogen peroxide with chemoselective fluorescent probes," *Journal of Biomedical Optics,* vol. 18, no. 10, p. 106002, 2013.

[8] M. V. Avshalumov and M. E. Rice, "Activation of ATP-sensitive K+ (KATP) channels by H2O2 underlies glutamate-dependent inhibition of striatal dopamine release," *Proceedings of the National Academy of Sciences of the United States of America,* vol. 100, no. 20, pp. 11729-11734, 2003.

[9] M. V. Avshalumov, B. T. Chen, S. P. Marshall, D. M. Pena, and M. E. Rice, "Glutamate-dependent inhibition of dopamine release in striatum is mediated by a new diffusible messenger, H_2O_2," *Journal of Neuroscience,* vol. 23, no. 7, pp. 2744-2750, 2003.

[10] M. V. Avshalumov, B. T. Chen, T. Koos, J. M. Tepper, and M. E. Rice, "Endogenous hydrogen peroxide regulates the excitability of midbrain dopamine neurons via ATP-sensitive potassium channels," *Journal of Neuroscience,* vol. 25, no. 17, pp. 4222-4231, 2005.

[11] M. V. Avshalumov, J. C. Patel, and M. E. Rice, "AMPA Receptor-Dependent H2O2 Generation in Striatal Medium Spiny Neurons But Not Dopamine Axons: One Source of a Retrograde Signal That Can Inhibit Dopamine Release," *Journal of Neurophysiology,* vol. 100, no. 3, p. 1590, 2008.

[12] L. Bao *et al.*, "Mitochondria Are the Source of Hydrogen Peroxide for Dynamic Brain-Cell Signaling," *Journal of Neuroscience,* vol. 29, no. 28, pp. 9002-9010, 2009.

[13] C. R. Lee, J. C. Patel, B. O'Neill, and M. E. Rice, "Inhibitory and excitatory neuromodulation by hydrogen peroxide: translating energetics to information:

Inhibitory and excitatory neuromodulation by H_2O_2 ," *The Journal of Physiology,* vol. 593, no. 16, pp. 3431-3446, 2015.
[14] F. Antunes and E. Cadenas, "Estimation of H_2O_2 gradients across biomembranes," *FEBS Letters,* vol. 475, no. 2, pp. 121-126, 2000.
[15] N. M. Mishina *et al.*, "Does Cellular Hydrogen Peroxide Diffuse or Act Locally?," *ANTIOXIDANTS & REDOX SIGNALING,* vol. 14, no. 1, pp. 1-7, 2011.
[16] N. L. Strominger, R. J. Demarest, and L. Laemle, *Noback's Human Nervous System, Seventh Edition* (no. Book, Whole). DE: Springer Verlag, 2012.
[17] R. L. Albin, A. B. Young, and J. B. Penney, "The Functional anatomy of Basal Ganglia Disorders," *Trends in Neurosciences,* vol. 12, no. 10, pp. 366-375, 1989.
[18] A. D. Smith and J. P. Bolam, "The Neural network of the Basal Ganglia as revealed by the study of synaptic connections of identified neurons," *Trends in Neurosciences,* vol. 13, no. 7, pp. 259-265, 1990.
[19] C. Pacelli, N. Giguere, M. J. Bourque, M. Levesque, R. S. Slack, and L. E. Trudeau, "Elevated Mitochondrial Bioenergetics and Axonal Arborization Size Are Key Contributors to the Vulnerability of Dopamine Neurons," *Current Biology,* vol. 25, no. 18, pp. 2349-2360, 2015.
[20] R. D. M. Travasso, F. S. d. Aidos, A. Bayani, P. Abranches, and A. Salvador, "Localized Redox Relays as a Privileged Mode of Cytoplasmic Hydrogen Peroxide Signaling," *Redox Biology,* 2017.
[21] G. M. Whitesides, "The origins and the future of microfluidics," *Nature,* vol. 442, no. 7101, pp. 368-373, 2006.
[22] T. F. Jiao, Q. Q. Huang, Y. Xiao, X. H. Shen, J. X. Zhou, and F. M. Gao, "Electrochemiluminescent Detection of Hydrogen Peroxide via Some Luminol Imide Derivatives with Different Substituent Groups," *Journal of Chemistry,* vol. 2013, pp. 1-6, 2013.
[23] C. C. Hsu, Y. R. Lo, Y. C. Lin, Y. C. Shi, and P. L. Li, "A Spectrometric Method for Hydrogen Peroxide Concentration Measurement with a Reusable and Cost-Efficient Sensor," *SENSORS,* vol. 15, no. 10, pp. 25716-25729, 2015.
[24] C. Liu, M. G. Schrlau, and H. H. Bau, "Single bead-based electrochemical biosensor," *Biosensors and Bioelectronics,* vol. 25, no. 4, pp. 809-814, 2009.
[25] S. Chakraborty and C. R. Raj, "Pt nanoparticle-based highly sensitive platform for the enzyme-free amperometric sensing of H2O2," *Biosensors and Bioelectronics,* vol. 24, no. 11, pp. 3264-3268, 2009.
[26] M. I. GonzÁLez-SÁNchez, L. GonzÁLez-Macia, M. T. PÉRez-Prior, E. Valero, J. Hancock, and A. J. Killard, "Electrochemical detection of extracellular hydrogen peroxide inArabidopsis thaliana: a real-time marker of oxidative stress: Direct detection of H2O2in Arabidopsis thaliana," *Plant, Cell & Environment,* vol. 36, no. 4, pp. 869-878, 2013.
[27] S. J. Updike and G. P. Hicks, "The Enzyme Electrode," *Nature,* vol. 214, no. 5092, pp. 986-988, 1967.
[28] D. A. Walsh, K. R. J. Lovelock, and P. Licence, "Ultramicroelectrode voltammetry and scanning electrochemical microscopy in room-temperature ionic liquid electrolytes," *Chemical Society Reviews,* vol. 39, no. 11, pp. 4185-4194, 2010.

[29] X. Liu and J. L. Zweier, "A real-time electrochemical technique for measurement of cellular hydrogen peroxide generation and consumption: evaluation in human polymorphonuclear leukocytes," *Free Radical Biology and Medicine,* vol. 31, no. 7, pp. 894-901, 2001.

;) random emoji because it's 2018